Chapter 4
Cohesive Sediment Transport

Page

Chapter 4
Cohesive Sediment Transport

by
Jianchun Huang, Robert C. Hilldale, and Blair P. Greimann

4.1 Introduction

Cohesive sediments are composed primarily of clay-sized material, which have strong interparticle forces due to their surface ionic charges. As particle size decreases, its surface area per unit volume (i.e. specific surface area) increases, and the interparticle forces, not the gravitational force, dominate the behavior of sediment. There is no clear boundary between cohesive sediment and non-cohesive sediment. The definition is usually site-specific. In general, finer sized grains are more cohesive. Sediment sizes smaller than 2 μm (clay) are generally considered cohesive sediment. Sediment of size greater than 60 μm is coarse non-cohesive sediment. Silt ($2\mu m - 60\mu m$) is considered to be between cohesive and non-cohesive sediment. Indeed, the cohesive properties of silt are primarily due to the existence of clay. Thus in engineering practice, silt and clay are both considered to be cohesive sediment.

Cohesive sediments consist of inorganic minerals and organic material (Hayter, 1983). Inorganic minerals consist of clay minerals (e.g. silica, alumina, montmorillonite, illite, and kaolinite) and non-clay minerals (e.g. quartz, carbonates, feldspar, and mica, among others). The organic materials may exist as plant and animal detritus and bacteria.

Cohesive sediments are a concern in many waterways and are closely linked to water quality. Many pollutants, such as heavy metals, pesticides, and nutrients preferentially adsorb to cohesive sediments. In addition to the contaminants adsorbed to the sediments, the sediments themselves are sometimes a water quality concern. The turbidity caused by sediment particles can restrict the penetration of sunlight and decrease food availability, thus affecting aquatic life. Turbidity also increases water treatment costs.

4.2 Cohesive Sediment Processes

4.2.1 Aggregation

Cohesive sediments tend to bind together (aggregate) to form large, low-density units. This process is strongly dependent upon the type of sediment, the type and concentration of ions in the water, and the flow condition (Mehta et al. 1989). Metallic or organic coatings on the particles may also influence the interparticle attraction of fine sediments. Cohesive sediments are composed primarily of clay-sized material, which have strong interparticle forces due to their surface ionic charges. As particle size decreases, the interparticle forces dominate the gravitational force, and the settling velocity is no longer a function of only particle size. A predictive model of the aggregation process was formulated by McAnally and Mehta (2001) through a dimensional analysis of the significant parameters in collision, aggregation, and disaggregation.

In engineering models, aggregation is often indirectly considered by the change in settling velocity. The weight of an individual fine sediment particle is not sufficient to cause settling when the particle is suspended in water because any small disturbance, such as a turbulence fluctuation, will overcome the weight of the particle. The cohesion of the sediment causes the small particles to bind together to form larger flocs. The flocs may grow when they collide with other particles or other flocs. They may also be broken up by turbulent stress. The floc structure (size, density, and shape) determines the settling velocity. The effective settling rate is the fall velocity multiplied by a hindrance factor, which represents the velocity reduction due to other particles.

Krone (1962) performed flume studies and found that the settling velocity increases with sediment concentration and proposed the following formula:

$$\omega = KC_s^{4/3} \tag{4.1}$$

where ω = settling velocity (m/s),
C_s = suspended sediment concentration (g/l), and
K = an empirical constant equal to approximately 0.001 depending on the type of sediment.

A similar relationship was used by Cole and Miles (1983):

$$\omega = KC_s \tag{4.2}$$

where K = an empirical constant with a value of about 0.001 to 0.002.

Van Leussen (1994) proposed an empirical relationship between settling velocity, concentration and shear stress:

$$\omega = KC_s^n \frac{1+aG}{1+bG^2} \tag{4.3a}$$

where a, b = empirical constants, and
G = dissipation parameter defined as:

$$G = \sqrt{\frac{\varepsilon}{\nu}} \tag{4.3b}$$

where ε = turbulent energy dissipation rate, and
ν = molecular viscosity.

Nezu and Nakagawa (1993) provided the empirical relationship for ε in simple steady, uniform open channel flow as:

$$\varepsilon = \frac{u_*^3}{\kappa D}\frac{1-\zeta}{\zeta} \tag{4.3c}$$

where u_* = shear velocity,
κ = Von Kárman constant,
ζ = z/D, the relative elevation above the bed,
z = elevation above the bed, and
D = river depth.

The above relationships are not valid at high concentration. Thorn (1981) showed that the settling velocity increases with concentration at low concentration, then attains a maximum value and thereafter decreases due to hindered settling at intermediate concentrations and structural flocculation at large concentrations. Nicholson and O'Connor (1986) used the following relationship for settling velocity computation to incorporate these effects:

$$\begin{aligned} \omega &= A_1 C_s^{B_1}, & C_s \le C_H \\ \omega &= A_1 C_H^{B_1}[1.0 - A_2(C_s - C_H)]^{B_2}, & C_s > C_H \end{aligned} \tag{4.4}$$

where C_H = 25g/l refers to the onset concentration of hindered settling,
A_1 = 6.0×10^{-4} $m^4/kg/s$,
A_2 = 1.0×10^{-2} m^3/kg,
B_1 = 1.0, and
B_2 = 5.0.

All of the above coefficients are experimentally determined constants depending on the sediment type and salinity.

Burban et al. (1990) linked the settling velocity with the median floc diameter d_m from laboratory data:

$$\omega = a d_m^b \tag{4.5a}$$

with

$$a = B_1 (C_s \tau)^{-0.85} \tag{4.5b}$$

$$b = -[0.8 + 0.5\log(C_s \tau - B_2)] \tag{4.5c}$$

where C_s = cohesive sediment concentration (g/cm^3),
τ = fluid shear stress ($dyne/cm^2$),
d_m = median floc diameter (cm), and
B_1 and B_2 = 9.6×10^{-4} and 7.5×10^{-6}, respectively, both are experimentally determined constants.

Lick and Lick (1988) and Gailani et al. (1991) provided an experimentally based equation for determining the median floc diameter, written as:

$$d_m = (\frac{\alpha_o}{C_s \tau})^{1/2} \tag{4.5d}$$

where α_0 = experimentally determined constant (= 10^{-8} g-m^2/cm^3-s^2 in freshwater).

Thorn (1981) showed that the settling velocity increases with concentration when concentrations are low, then attains a maximum value and thereafter decreases due to hindered settling at intermediate concentrations and structural flocculation at large concentrations. Van Rijn (1993) summarized the influence of sediment concentration on the settling velocity for sediments all over the world (Figure 4.1). Some of these sediments are implemented in GSTAR-1D.

The settling velocities, due to sediment flocculating, are usually site-specific and need to be determined by experiment. GSTAR-1D allows the user to provide a set of user specified data as shown in Figure 4.2.

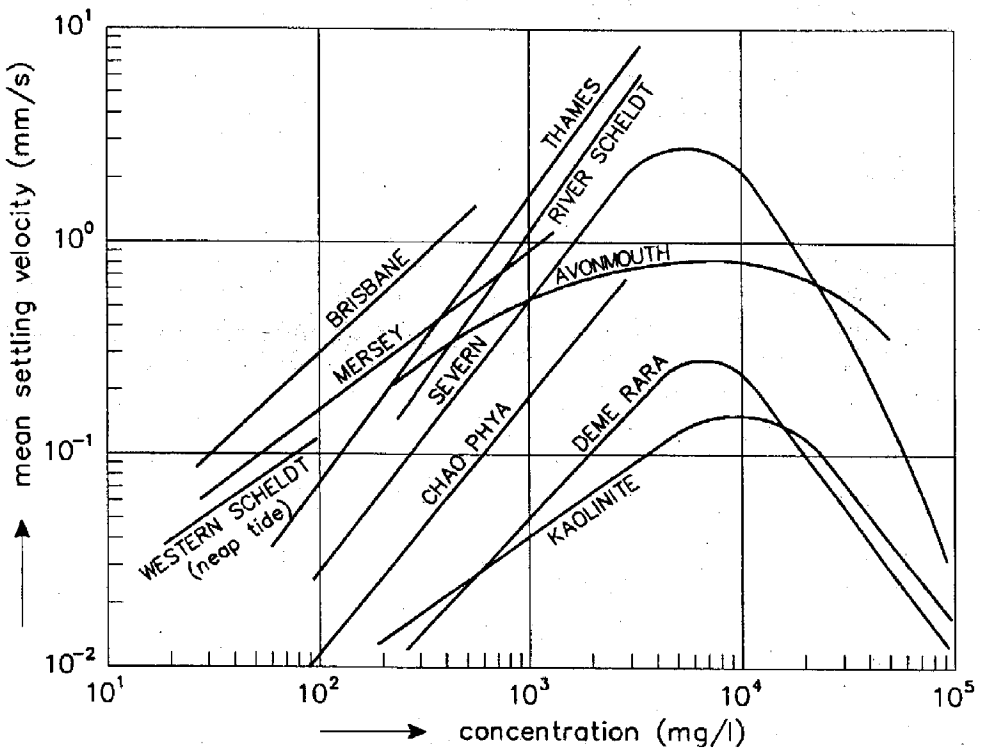

Figure 4.1. The influence of sediment concentration on the settling velocity (source: Van Rijn, 1993, Figure 11.4.2).

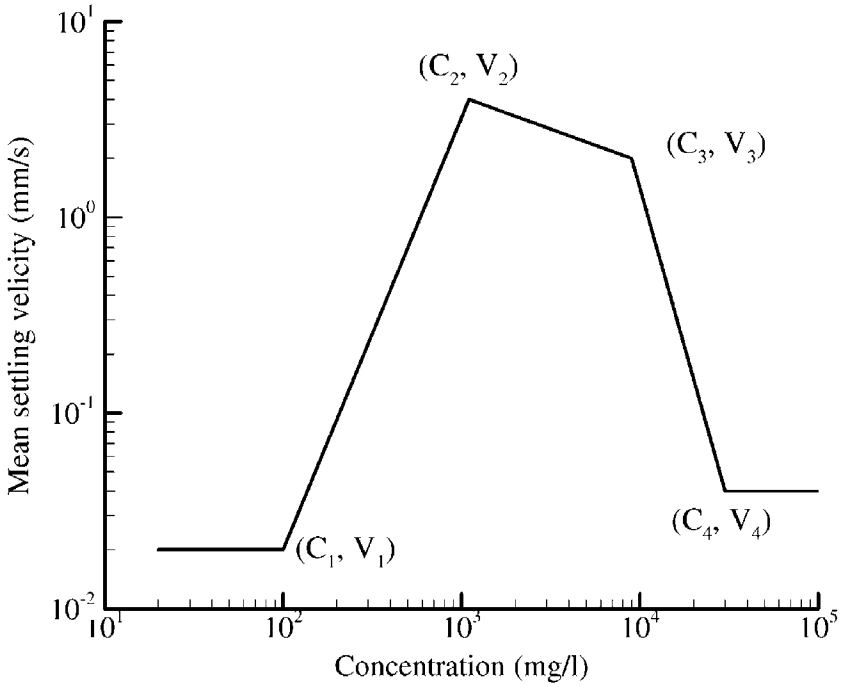

Figure 4.2. Input data illustration for settling velocity.

4.2.2 Deposition

Deposition occurs when the bottom shear stress is less than the critical shear stress. Only aggregates with sufficient shear strengths to withstand the highly disruptive shear stresses in the near bed region will deposit and adhere to the bed. Mehta and Partheniades (1973) performed laboratory studies on the depositional behavior of cohesive sediment and found that deposition is controlled by the bed shear stress, turbulence processes in the zone near the bed, settling velocity, type of sediment, depth of flow, suspension concentration and ionic constitution of the suspending fluid (also summarized in Hayter et al., 1999).

Two kinds of sediment deposition are included in GSTAR-1D, full and partial deposition. When the bed shear stress (τ) is smaller than the critical shear stress for full deposition ($\tau_{d,full}$), all sediment particles and flocs are deposited. Krone's (1962) deposition formulation is

$$Q_d = P_d \omega c \qquad \text{for } \tau \le \tau_{d,full} \tag{4.6a}$$

where Q_d = deposition rate, and
P_d = the deposition probability.

The variable P_d is also the probability of particles sticking to the bed and not being re-entrained by the flow. A fraction of sediments settling to the near bed region cannot withstand the high shear stresses at the sediment-water interface and are broken up and re-suspended. The probability of deposition is given by

$$P_d = 1 - \tau / \tau_{d,full} \qquad \text{for} \qquad for \quad \tau \le \tau_{d,full} \tag{4.6b}$$

where τ = bottom shear stress, and
$\tau_{d,full}$ = critical shear stress for full deposition.

Many experiments were preformed to determine the values of critical shear stress for full deposition of cohesive sediments. They range between 0.06 and 1.1 N/m^2 depending upon the sediment type and concentration. Krone (1962) conducted a series of flume experiments to determine the critical shear stress for full deposition. For San Francisco Bay sediment, he found that $\tau_{d,full}$ = 0.06 N/m^2 when c < 0.3g/l; $\tau_{d,full}$ = 0.078 N/m^2 when 0.3 < c < 10g/l. Mehta and Partheniades (1975) found that $\tau_{d,full}$ = 0.15 N/m^2 for kaolinite in distilled water.

Partial deposition exists when the bed shear stress is greater than the critical shear stress for full deposition but smaller than the critical shear stress for partial deposition. At this range of bed shear stress, relatively strong flocs are deposited and relatively weak flocs remain in suspension. The partial deposition formulation is written as

$$Q_d = P_d \omega (c - c_{eq}) \quad \text{for} \qquad \tau_{d,full} < \tau < \tau_{d,part} \tag{4.6c}$$

where c_{eq} = equilibrium sediment concentration.

The equilibrium sediment concentration is the concentration of relatively weak flocs that do not have sufficiently strong bonds and will be broken down before reaching the bed or will be eroded immediately after being deposited. The probability of deposition is given by

$$P_d = 1 - \tau / \tau_{d,part} \quad \text{for} \qquad \tau_{d,full} < \tau < \tau_{d,part} \tag{4.6d}$$

There is no deposition when the bed shear stress is larger than the critical shear stress for partial deposition. The deposition rate is zero,

$$P_d = 0 \qquad \text{for} \qquad \tau \ge \tau_{d,part} \tag{4.6e}$$

At present, the behavior of critical shear stresses for full and partial depositions are not well understood, but the accuracy of the deposition model mainly depends on the use of their correct values. Thus, when the actual value of $\tau_{d,full}$ and $\tau_{d,partl}$ are uncertain, they become primary calibration parameters for determining the deposition rate.

4.2.3 Consolidation

Consolidation is another important phenomena in cohesive sediment transport. Two types of consolidation are usually considered: primary and secondary (Mehta et. al, 1989). Primary consolidation is caused by the self-weight of sediment, as well as the deposition of additional materials. Primary consolidation begins when the self-weight of the sediment exceeds the seepage force induced by the upward flow of pore water from the underlying sediment. During this stage, the self-weight of the particles expels the pore water and forces the particles closer together. The seepage force lessens as the bed continues to undergo self-weight consolidation. Primary consolidation ends when the seepage force has completely dissipated. Secondary consolidation is caused by the plastic deformation of the bed under a constant overburden. It begins during the primary consolidation and may last for weeks or months.

The consolidation process is incorporated into engineering models by representing the bed with a number of layers, each having a specific thickness, consolidation time, and critical shear stress. An idealized version of the consolidation process models the relationship by linking the layer bulk density, ρ, to the consolidation time, t (Nicholson and O'Connor, 1986):

$$\rho_b = \begin{cases} \rho_f, & t \le t_f \\ \rho_f + (\rho_\infty - \rho_f)\{1.0 - \exp[-A_2(t - t_f)]\}^{B_2}, & t_f < t < t_\infty \\ \rho_\infty, & t \ge t_\infty \end{cases} \tag{4.7}$$

where ρ_b = dry bulk density,
t = time, and
A_2 and B_2 = coefficients that account for the influence of mud type and salinity.

The subscripts f and ∞ represent the freshly deposited and the fully consolidated states, respectively.

Nicholson and O'Connor (1986) adopted the following values (Table 4.1) for the Grangemouth Harbor in Scotland, however the values of t_f, t_∞ and A_2 were not given.

Table 4.1. Model consolidation parameters of Nicholson and O'Connor

Consolidation parameter	Value
ρ_f	80 kg/m^3
ρ_∞	300 kg/m^3
B_2	0.45

Another similar consolidation model was applied by Teisson and Latteux (1986) in the Loire Estuary. The bed profile is considered to be composed of a number of layers of various thickness, each with a specified density, resistance to fluid shear, and duration of deposition. The bulk density for the Loire Estuary is given by:

$$\rho_b = \begin{cases} 136.2\log_{10}(t+5.42), & 0 < t \le 24h \quad t \text{ in hours} \\ 200+70\log_{10}(t), & t > 1 \text{ day} \quad t \text{ in days} \end{cases} \tag{4.8a}$$

Furthermore, they related the critical shear velocity for erosion to bed bulk density by,

$$u_{*_e} = \begin{cases} 3.2\times10^{-5}\rho_b^{\,1.175}, & \rho_b < 240g/l \\ 5.06\times10^{-8}\rho_b^{\,2.35}, & \rho_b > 240g/l \end{cases} \tag{4.8b}$$

With these relationships, their consolidation model uses the values shown in Table 4.2.

Table 4.2. Consolidation model values

Layer	Density (g/l)	Duration	u_{*_e} (cm/s)
1	100	2 hours	0.72
2	120	4 hours	0.88
3	145	8 hours	1.11
4	175	16 hours	1.38
5	205	1day 8 hours	1.66
6	230	2 days 16 hours	1.91
7	250	5 days 8 hours	2.18
8	270	10 days 16 hours	2.62
9	290	infinite	3.10

Another consolidation model was applied in the computer model SED2D WES (Letter et al., 2000) where the change in density with time is governed by the following equation:

$$\rho = \rho_f - (\rho_f - \rho_i)e^{-\beta t} \tag{4.9a}$$

where ρ = time-varying density,
ρ_i = initial density,
ρ_f = final ultimate density,
t = time, and
β = consolidation coefficient in 1/sec.

The consolidation coefficient β is calculated from user input for initial density and density at the reference time by solving Equation (4.9a):

$$\beta = \frac{1}{t_e}\ln\frac{\rho_f - \rho_i}{\rho_f - \rho_e} \tag{4.9b}$$

where ρ_e = density at reference time t_e.

4.2.4 Toxicant Adsorption and Desorption

Many pollutants, such as heavy metals, pesticides, and nutrients preferentially adsorb to cohesive sediments. Cohesive sediment serves as a carrier for toxicants, strongly relating water quality to cohesive sediment transport. Toxicants can be adsorbed onto sediment surfaces as adsorbed toxicants, and can be dissolved in the water as dissolved toxicants (adsorbed phase and dissolved phase). Adsorption is defined as the toxicants adhering to suspended sediments from the dissolved phase. Adsorbed toxicants can be removed from the water column after the cohesive sediment is deposited onto the river bed. Desorption is defined as the toxicant becoming dissolved in the water after being removed from the sediment surface. This usually happens when contaminated sediment is eroded from the river bed. Experiments (Thomann and DiToro, 1983) show that equilibrium between the dissolved and adsorbed phases is attained within minutes. Instantaneous local equilibrium is assumed for engineering problems.

Shrestha and Orlob (1996) presented a two-dimensional (2D) numerical model to simulate the fate and transport of cohesive sediments and associated nickel in southern San Francisco Bay. A partition coefficient, K_p, is used to define the distribution of the toxicant between the adsorbed and dissolved phases. The partition coefficient (m^3/kg) is defined as,

$$K_p = \frac{C_p}{C_d C_s} \tag{4.10}$$

where C_p = adsorbed toxicant concentration by weight (kg/m^3),
C_d = dissolved toxicant concentration by weight (kg/m^3), and
C_s = sediment concentration by weight (kg/m^3).

The partition coefficient for each toxicant is usually site-specific, and can be determined in the laboratory or in the field. The fraction of toxicant in the adsorbed phase, f_p is written as:

$$f_p = \frac{C_p}{C_t} = \frac{k_d C_s}{1 + k_d C_s} \tag{4.11}$$

where C_t = total toxicant concentration by weight (kg/m^3), and
k_d = equilibrium distribution coefficient (m^3/kg).

The sorbed mass of toxicant per unit mass of sediment is:

$$\frac{C_p}{C_s} = \frac{f_p C_t}{C_s} \text{ (kg/kg)} \tag{4.12}$$

If ΔM is the total mass of sediment deposited per unit area (kg/m^2) during a specific time period, then the toxicant mass associated with the deposited sediments is:

$$\Delta M_p = \frac{f_p C_t}{C_s} \Delta M \quad (\text{kg/m}^2) \tag{4.13}$$

On the other hand, the erosion of sediment brings toxicants back into the water column. If ΔM is the total mass of sediment eroded per unit area (kg/m^2) during a specific time period, then toxicant mass associated with the eroded sediment is:

$$\Delta M_p = \frac{f_p C_{t,b}}{C_{s,b}} \Delta M \quad (\text{kg/m}^2) \tag{4.14}$$

where $C_{s,b}$ = sediment concentration in bed (kg/m^3), and
$C_{t,b}$ = concentration of toxicant adsorbed to sediment in bed (kg/m^3).

4.2.5 Erosion

This section will address the major factors influencing a soil's ability to resist erosion, experimental methods to determine erodibility and a discussion on erosion parameters and formulae. Erosion of cohesive soils in this section refers to surface erosion (or fluvial or particle erosion), whereby individual particles or small aggregates are removed from the soil mass by hydrodynamic forces such as drag and lift (Millar and Quick, 1998). The ability of a cohesive soil to resist surface erosion is known as erosional strength (Zreik et al., 1998). Resistance to surface erosion differs from resistance to mass erosion. Mass erosion is determined by the soil's undrained strength, or yield strength (Millar and Quick, 1998). Mass erosion occurs when the yield strength is exceeded such as a slip failure of a streambank or when large flakes or chunks of soil are eroded from the streambed. Studies have shown (Kamphuis and Hall, 1983; Zreik et al., 1998; and Hilldale, 2001), that there is a strength difference of one to three orders of magnitude between erosional strength and yield strength.

Due to the complex and widely varied nature of particle bonds, much less is known about the properties influencing the bonding of cohesive soils. Unlike coarse sediments, cohesive sediments are not amenable to classification by grain size and distribution. These complex bonds greatly complicate modeling efforts of deposition and resuspension criteria for streams with a cohesive bed and/or banks. Table 4.3 shows the list of 28 parameters (Winterwerp, et al., 1990) that is used by Delft Hydraulics to characterize cohesive sediments. In addition to the physical and electro-chemical effects influencing cohesive soil behavior, recent research has indicated that biological effects also have considerable influence on cohesive sediment processes. Sometimes biological factors may be more important than the electrochemical effects when determining cohesive strength (Paterson, 1994). With this vast number of parameters affecting soil properties it is expected that there may be an interaction between the electro-chemical and biological effects. For example an electro-chemical process known to influence compaction of the bed may be disrupted by the presence of benthos.

Table 4.3. List of parameters used in the MAST-1 G6M project to characterize mud. This is a tentative list, resulting from the combination of the different lists used by the participants of the MAST G6M Cohesive Sediment Project. Some parameters are interdependent (after Winterwerp et al., 1990). Biological effects not included

Physico-chemical properties of the overflowing fluid	(19) specific surface
(1) chlorinity	(20) mineralogical composition
(2) temperature	(21) grain size distribution and sand content
(3) oxygen content	**Characteristics of bed structure**
(4) redox potential	(22) consolidation a. consolidation curve and density profile b. permeability c. pore pressure and effective stress
(5) pH	
(6) Na-, K-, Mg-, Ca-, Fe-, Ai- ions	
(7) sodium adsorption ratio (SAR)	
(8) suspended sediment concentration	(23) rheological parameters a. upper and lower yield stress b. Bingham viscosity c. equilibrium slope of mud deposits
Physico-chemical properties of the mud	
(9) chlorinity	
(10) temperature	
(11) oxygen content	(24) Atterberg limits (liquid and plastic limit)
(12) redox potential	**Water – bed exchange processes**
(13) pH	(25) settling velocity a. as a function of sediment concentration and floc density b. as a function of salinity
(14) gas content	
(15) organic content	
(16) Na-, K-, Mg-, Ca-, Fe-, Ai- ions	(26) critical shear stress for deposition
(17) cation exchange capacity (CEC)	(27) critical shear stress for erosion
(18) bulk density (density profile)	(28) erosion rate

4.2.5.1 Physical Factors Affecting Erodibility

Physical parameters affecting erodibility include: clay content, water content, clay type, temperature, bulk density (largely a reflection of the age of the deposit) and pore pressure, (Winterwerp et al., 1990). These properties vary greatly from one site to another. Rarely is a soil entirely made up of clay particles, rather fine sand and silt often make up a significant portion of the soil. For soils containing more than approximately 10% clay, the clay particles will assume control of the soil properties (Raudkivi, 1998). For a comprehensive discussion of the physical properties and minerology of the various types of clay particles, readers should refer to Loose Boundary Hydraulics, Chapter 10 (Raudkivi, 1998).

4.2.5.2 Electrochemical Factors Affecting Erodibility

The chemistry of the eroding fluid and the pore fluid influences the valence of clay particles and therefore plays a critical role in interparticle bonding. For example, increasing the electrolyte concentration or changing the cations in the pore fluid of a clay to one of a higher valence tends to cause flocculation of a clay–water suspension (Verwey and Overbeek, 1948). The Cation Exchange Capacity (CEC) is a measure of the type and amount of clay and is defined as the number of milliequivalents of exchangeable cations per 100 grams of dry soil. Increasing values of CEC have been shown (Ariathurai and Arulanandan, 1978) to decrease the erosion rate. In addition to the effects of cations and electrolytes, the pH of the pore fluid in the sediment matrix provides a significant contribution to the strength of the interparticle bond. Ravisanger et al. (2001) reported the following results on the effects that pH levels have on particle orientation and interparticle forces of kaolinite. The pore fluid pH influences the particle orientation during bonding by changing the surface or edge charges of the particles. These particle orientations are Edge-Edge (E-E), Edge-Face (E-F) and Face-Face (F-F). Briefly, low pH values ($pH \leq 5.5$) cause predominantly E-F associations, resulting in a stratified sediment bed exhibiting high erosion rates near the surface. Once the surficial sediments are eroded the erosion rate tends to become a relatively constant value. Intermediate pH conditions ($5 \leq pH \leq 7$) result in a reorientation of the bed structure from E-F to E-E particle associations. This results in a weaker bed structure due to the lack of surface contact, causing the bed to be more susceptible to erosion. At higher pH values ($pH > 7$) F-F particle orientations predominate and surface attraction forces of become significant because the area of surface contact has greatly increased, forming denser aggregates. This type of soil is fairly resistant to erosion.

Another significant factor in soil strength is salinity. The total content of dissolved salts in the pore fluid is a main factor in the susceptibility of cohesive soils to erosion (Sherard et al., 1972). These same authors also reported that the ratio of dissolved sodium ions to the other main basic cations (calcium and magnesium) in the pore water governs the susceptibility of cohesive soils to erosion. This is known as the Sodium Adsorption Ratio (SAR) and Arulanandan et al., (1975) showed that decreasing values of SAR decreased the erosion rate.

The presence of natural organic matter (NOM) in the eroding fluid is a result of decaying aquatic plant and animal matter (Schnitzer and Khan, 1972 and Thurman and Malcolm, 1983). Natural organic matter is measured as a percent of organic carbon adsorbed to the clay particles in the soil (Dennett et al., 1998). Adsorbed NOM can significantly affect the behavior of clay particles by influencing the interparticle bonding (Bennett, et al., 1991). Flume tests by Dennett et al. (1998) in which the level of NOM (% carbon) varied from 0.0% to 0.12% show an increased resistance to erosion with an increase in NOM. For the purpose of this discussion, the influence of NOM is not considered a biological effect due to the fact that living organisms are not directly involved the process.

4.2.5.3 Biological Factors Affecting Erodibility

The effects of organisms inhabiting stream or estuarial sediments may have three potential influences on the erodibility of the sediments; neutral (no effect), negative (decreasing soil

stability) or positive (increasing soil stability). A positive effect on sediment stability is described as biogenic stabilization or biostabilization. This term has been defined as "a decrease in sediment erodibility caused directly or indirectly by biological action" (Paterson and Daborn, 1991). One of the most common negative effects of biological action is the reworking of the sediment by organisms known as bioturbation (a reworking or packaging of the sediment bed by organisms) (Paterson, 1997).

One way in which biogenic effects influence sediment stability is the growth of organisms on the bed surface (Paterson, 1997). The entrainment of particles is generally related to the hydrodynamic forces of drag and lift. Uneven surfaces with protrusions create a condition of hydraulic roughness. As organisms grow they have an effect of smoothing the bed by filling the inter-particle voids or creating a microbial mat (Manzenrider, 1983), reducing the hydraulic roughness. This decreases the stress in the near bed region having the effect of strengthening the bed by effectively increasing the velocity for which particles are entrained (Paterson, 1997).

It has been shown by Paterson (1997) that discrete particles (glass beads in this case) can become cohesive by the growth of bacteria and diatoms. The particles become covered with the developing growth of the bacteria and diatoms, causing cohesion to increase and roughness to decreases. Further binding is provided by bacterial secretion known as extracellular polymeric substances (EPS) forming cohesive networks between the diatoms. This biostabilization of originally non-cohesive particles points to the significant effect of biological processes.

Burrowing organisms have been shown to have both positive and negative effects on the stability of surficial soils. Laboratory research by Brekhovskikh et al. (1991) shows a possible 10-fold decrease in the critical stress for erosion when Oligochaeta (common burrowing worms in fresh water environments) are present. These effects were shown to largely depend on the population density and temperature. The same researchers found that Chironomids (common midges with burrowing larva in fresh water and sometimes saline environments) also had a negative effect on sediment stability; however, that influence decreased over time as the organisms excreted mucus and developed tube houses, cementing the bed and making it less erosive (the net effect was still negative because erosion was still less in the control flume).

Other research by Meadows et al. (Meadows and Tait, 1985 & 1989; Meadows et al., 1991; and by Meadows and Meadows, 1991) shows a strengthening of the bed by burrowing organisms. This work has demonstrated the potential of burrowing organisms to locally increase the critical shear stress of sediments. Results obtained by Black (1997) show the phenomenon of benthic adhesion within estuarine muds as a predominating influence over well documented electro-chemical particle-particle interactions. Black's (1997) research also indicated a positive effect of benthic diatoms by increasing inter-bond strength through the secretion of adhesive carbohydrate-rich mucus. It is likely that the effects of burrowing organisms and benthic diatoms are somewhat dependant on the soil type in addition to other site-specific conditions (e.g. salinity, pH, temperature).

A study (Littoral Investigation of Sediment Properties (LISP)-89, as reported in Daborn, 1993) performed by more that 30 scientists was carried out in a tidal flat to determine the threshold parameters for a numerical model. The critical shear stress was considered the essential parameter of this investigation. During this investigation it was found (Amos et al., 1988) that the sediment surface became significantly more resistant to erosion during the late summer. These results were obtained using an in-situ flume known as Sea Carousel. It was noted that several biological changes were occurring at the same time. During the investigation the foraging amphipod *Corophium volutator* was seen actively crawling at the soil surface (Boates and Smith, 1988). This foraging amphipod grazes on epipelic diatoms during ebbing tides. The diatoms have been shown by poisoning experiments and Sea Carousel flume measurements (Daborn, 1993) to increase the soil strength through secretions of soluble carbohydrates. The disappearance of *Corophium volutator* coincides with the arrival of migratory shore birds, which feed selectively on *Corophium* at rates estimated to be greater than 10,000 *Corophium* per bird per day (Hicklin and Smith, 1984). Daborn (1993) reports that more than 100,000 birds were in the estuary at their peak. With the arrival of the birds the numbers of the *Corophium* decreased and so did their behavior. The *Corophium* no longer grazed the surface but remained in their burrows to avoid predation (Boates and Smith, 1988). The conclusion reached by Daborn (1993) is that the decline of the *Corophium* activity produces greater amounts of chlorophyll, carbohydrates and organic matter in the soil due to the increased numbers of benthic diatoms. This has a secondary effect of increasing the soil's resistance to erosion.

The general conclusion of the studies mentioned above is that there is no comprehensive method to determine cohesive soil erodibility based solely on the known parameters of individual soils. Each site has specific physical, chemical and biological factors affecting the strength of the soil with no two being identical. Moreover, seasonal changes are likely to affect the presence of biota, since many of these species can not survive in low water temperatures. To successfully apply a numerical model of cohesive streambeds, it is necessary to test the individual soils for threshold conditions of erosion and deposition.

4.2.6 Experimental Methods to Determine Erosion Parameters

With the vast number of factors involved in the determination of the erodibility of cohesive soils, it becomes necessary to test cohesive soils for critical shear stress for erosion and deposition rather than using soil properties for predicting threshold values or using methods similar to those for coarse sediments. Some investigators create a sediment bed in the laboratory through settling of a premixed slurry or a placed bed using a rebuilt soil. This method generally simulates young soil deposits and also provides control over parameters such as bed sediment concentration (bulk density), soil type, and water quality (e.g. salinity, pH and electrolyte concentration). Since these types of experiments use a highly disturbed soil, critical parameters including chemistry and biology are often unaccounted for. Testing 'undisturbed' soil deposits will likely incorporate the chemical and biological effects. However this is a difficult task when one considers that any disturbance to the sample will potentially lead to biased results. Obtaining a completely undisturbed sample of a cohesive soil is unlikely; however, it is possible to minimize the disturbance to the sample. For example, transporting and storing cohesive soil samples in their

natural water will not only prevent desiccation and minimize vibration during transport, but it also retains the chemical and biological properties that are instrumental in determining the soil's strength. Even if all the soil properties are retained for testing of an 'undisturbed' soil sample it is not likely that using the natural stream water is feasible, making it necessary to try to duplicate the chemical properties of the natural water (e.g. pH, temperature, salinity, electrolyte concentration, etc.). When one considers the uncertainties of extrapolating lab results to natural conditions, a strong case is made for in-situ testing of cohesive soils for threshold values. Recent investigators (e.g. Gust and Morris 1989, Black 1997, Ravens and Gschwend 1999) have used in-situ flumes to test soils in their natural environment. This seems to be the most promising method for determining the erodibility of cohesive soils.

Figure 4.3 illustrates an idealized graph of erosional and depositional characteristics determined from physical tests. In general, a physical test should provide erosion rates and critical shear stresses for deposition, surface erosion, and mass erosion. It should be mentioned that some test results are difficult to analyze due to wide scatter in data because of the inconsistent nature of cohesive soils.

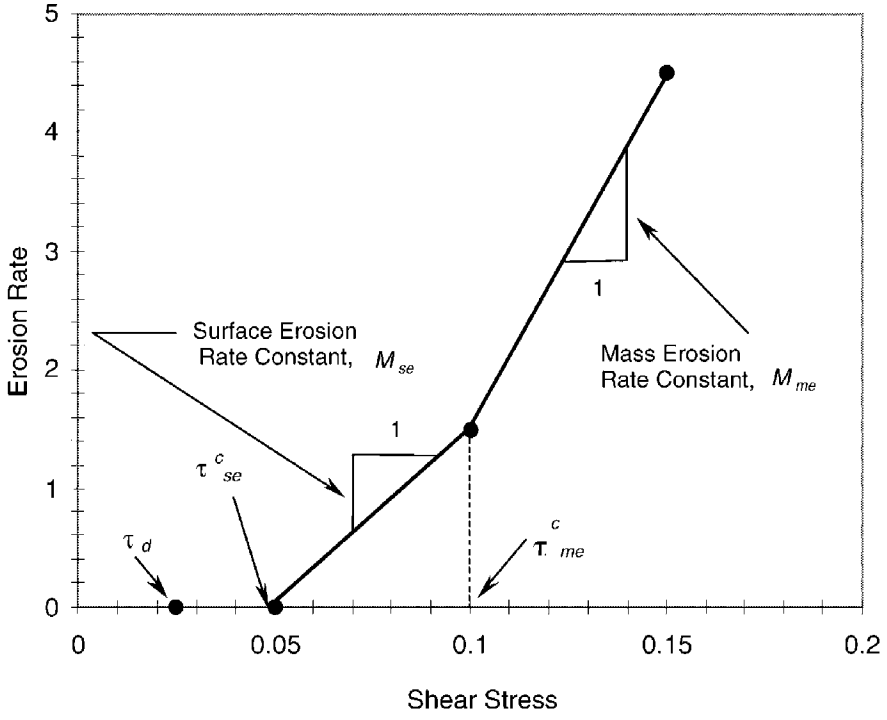

Figure 4.3. This idealized schematic illustrates the erosional characteristics that need to be determined from erosion tests and how they are plotted (after: Vermeyen, 1995). The values of critical shear stress for surface erosion (τ^c_{se}), critical shear stress for mass erosion (τ^c_{me}) and the subcritical condition of deposition (τ_d) is shown along with the mass and surface erosion rates. Units are intentionally omitted.

In the following sections (4.4.1 – 4.4.4), some common methods used to determine the erosion parameters of cohesive sediments are reviewed. These methods include the rotating cylinder, straight flume, annular flume, and in-situ testing methods.

4.2.6.1 Rotating Cylinder

A rotating cylinder used by Arulanandan et al. (1975) at the University of California at Davis is similar to the one developed by Masch et al. (1963). This device consists of two concentric cylinders separated by an annular space of 0.5 inches (1.27 cm). A soil sample 3.2 in. (8.13 cm) long and 3.0 in. (7.62 cm) in diameter is placed inside a Plexiglas cylinder that can be rotated at speeds up to 1500 rpm while the inner cylinder is stationary. The annular space is filled with an eroding fluid for the purpose of transmitting shear, creating a unidirectional current simulating stream flow. Stress on the soil is assumed to be nearly uniform due to a constant spacing between the soil and the outer cylinder and a uniform soil surface. This unidirectional flow around the soil cylinder created by this set-up can be described by the Navier-Stokes equations. The applied shear stress is calculated by the torque transmitted from the outer cylinder to the stationary inner cylinder. The erosion rate is determined by weighing the sample before and after each test to provide mass per unit time eroded from the sample for increasing values of shear stress. The erosion rate is plotted against the applied shear stress and the intercept on the applied shear stress axis defines the critical value. Results from Arulanandan et al., (1975) using the rotating cylinder are discussed later in this chapter.

A distinct advantage of this method is that the small volume of eroding fluid required allows for controlled conditions. Simulating, or actually using, natural stream water is possible. Altering the chemical composition of the eroding fluid to simulate the natural eroding fluid or varying a certain parameter is also possible since there is not a large volume of fluid involved. A similar device was used by Chapuis and Gatien (1986) to test intact samples without remolding. One drawback of an intact sample is the assumption of a smooth soil surface in determining a uniform shear stress. This assumption is valid for pure, remolded samples. However roots and/or larger discrete particles may protrude from the surface when a natural sample is used. This creates areas of locally increased shear stress, for which it is difficult to account. Chapuis and Gatien (1986) advise not cutting the sample with a thin-walled tube, stating that the surface of the sample becomes scaled due to surface remolding. These authors recommend a steel template and wire device to carve the sample.

4.2.6.2 Straight Flume Studies

Straight flumes have been used by many investigators (Vermeyen 1995; McNeil et al. 1996; Dennett et al., 1998 and Hilldale 2001) to determine the initiation of motion of cohesive sediments. Straight flumes allow the placement of 'undisturbed' or rebuilt soil samples in the bed of the flume to simulate stream flows over a soil bed. Straight flumes can present specific problems when testing cohesive sediments. Testing deposition is difficult and would ideally require a very long flume with a continuous soil bed and varied slopes to create erosional and depositional conditions. Recirculating pump systems can shear the suspended material due to the

turbulence generated within the pumps, resulting in reduced floc sizes (Vermeyen, 1995) and making deposition experiments difficult to accurately duplicate. Maintaining conservation of mass for the soil is not likely in a recirculating system because soil may be deposited in pipe networks or the sump.

Hilldale (2001) used a recirculating flume with dimensions of 7.9 ft. long x 0.5 ft wide x 1.0 ft deep (2.4 m x 0.15 m x 0.31 m) to test the erosion criteria of cohesive bank soils. This system incorporated a tray containing an 'undisturbed' soil sample that was flush with the flume bed, which was built up with lead beads to create roughness upstream and downstream of the soil sample. This minimized fluid acceleration over the soil sample, which could skew results. To avoid edge effects, the soil sample did not extend the width of the flume. The soil sample was placed far enough downstream from the inlet so that the flow became fully developed before reaching the upstream edge of the soil sample. To test sediment entrainment, the fluid was sampled just downstream of the soil tray and compared to fluid samples taken upstream of the sample. When the downstream concentration was greater than the upstream (background) concentration, erosion was considered to have occurred. The uniform flow formula ($\tau = \rho gHS$) was used to calculate the applied shear stress over the sample. Dennett et al. (1998) found that determining shear stress using the uniform flow formula agreed with the slope of the logarithmic, near-bed velocity profile for similar test conditions. Several soil samples were tested varying the applied shear stress. The critical shear stress for erosion was determined from a plot of applied shear stress versus change in concentration. The applied shear stress at which the change in concentration increased from a zero value was determined to be the critical shear stress. No erosion rate was determined in this series of tests.

Vermeyen (1995) also tested an 'undisturbed' soil sample in a rectangular flume 12 ft. long x 0.96 ft. wide x 1.5 ft. deep (3.7 m x 0.29 m x 45.7 m). Two soil samples were placed end-to-end and were each 2.0 ft. (0.61 m) long and the full width of the flume. Erosion and deposition rates were quantified by measuring the sample's submerged weight. Velocity profiles were taken using an Acoustic Doppler Velocimeter (ADV) and shear stress was determined from the slope of the logarithmic velocity curve near the bed. The erosion rate and critical shear stress for erosion were determined following the method of Arulanandan et al. (1975). Deposition was also tested and quantified by weighing the sample before and after each test, which was run for a given amount of time.

Straight flumes incorporating similar processes have also been used by Westrich et al. (1997) and Kamphuis and Hall (1983). In the flume used by Westrich et al. (1997) sediment eroded by the fluid was monitored with a laser system placed just downstream of the sediment sample. Kamphuis and Hall (1983) used a flume tunnel capable of near bed flow velocities of 11.5 ft/s (3.5 m/s). Remolded soil samples were removed from the flume upon completion of the tests and evaluated.

Another straight flume method developed by McNeil et al. (1996) uses an innovative approach for exposing soil to the flow in order to examine the erodibility of natural soil deposits with depth. A straight, recirculating flume known as Sedflume (Sediment Erosion at Depth Flume) was designed and constructed to test undisturbed and reconstructed soil samples. This flume has

a test section with an open bottom through which a rectangular coring tube 3.9 in. x 5.9 in. (10 cm x 15 cm) containing sediment can be attached. As the sediment erodes from the surface of the core, a piston inside the core can be raised to keep the sediment sample flush with the flume bed. The soil is sampled in rectangular cores taken from the river bottom, which are attached to the test section of the flume. The soil was sampled in soft deposits by pushing the core into the sediment bed. For deeper and/or more compact deposits a Vibracoring head was used to work the sample tube into the soil. Duplicate cores to those tested in the flume were tested for the sediment bulk properties, particle size distributions and total organic carbon. These 'undisturbed' samples of soil were tested for the erosion rate by measuring the depth of sediment eroded during the time of the test. A plot of the erosion rate versus depth was obtained. The critical shear stress for erosion was also evaluated by Sedflume on reconstructed soil samples, aged in the coring tube. This condition was identified visually, rather than measured quantitatively, which most likely resulted in a critical value for mass erosion.

4.2.6.3 Annular Flume

Annular flumes have long been used for testing cohesive soil properties (e.g. Partheniades et al., 1966; Mehta and Partheniades 1973; Fukuda and Lick 1980; Sheng 1988; Delo 1988; Maa 1989, and Krishnappan 1993). These flumes are of various diameters (3 to 22 ft, (1 – 7 m)) and have rectangular cross sections. A lid is placed in such a way so it just comes into contact with the water surface. Both lid (or ring) and flume are rotated in opposite directions to create a channel velocity. By rotating the ring and flume in opposite directions significant secondary currents are avoided in the corners of the channel (Krishnappan, 1993). These secondary currents have been reported to be as high as 15% of the tangential velocity, which exceeds that of the settling velocity of clay suspensions (Maa, 1989). These flumes are often equipped with Plexiglas windows for viewing and taps for extraction of fluid to test suspended sediments. Velocity distributions and applied shear stresses can be determined by using a laser and Preston tube to calculate velocity profiles and applied shear stresses, respectively, in clear water flows without sediment in the flume (Krishnappan, 1993). This data was obtained for various rotation speeds of the flume and lid. Suspended sediment is sampled from taps in the side of the flume and filtered to determine concentration. Zreik et al. (1998) used an annular flume and reported results in graphs of concentration versus time. These charts show rapid increases immediately after each incremental increase of shear stress. These same authors also report bed age, shear stress, test duration, erosion depth and temperature for each test performed.

The sediment bed of an annular flume can be prepared in a number of ways. For example Zreik et al. (1998) created the bed by allowing deposition of Boston Blue Clay from suspension in distilled water (prepared ahead of time). This procedure was followed by mixing the suspension by rotating the flume and followed by quiescent settling and aging of the bed for a specified amount of time, depending on the condition to be tested. Brekhovskikh et al. (1991) prepared the soil bed before adding water for the purpose of creating a soil bed containing benthos. Annular flumes provide a distinct advantage over straight flumes for testing deposition of cohesive soils. Fragile aggregates are not subject to break-up by pump propellers and do not settle in unwanted portions of the flume (e.g. headbox or pipes) as is the case in straight flumes. However annular

flumes are not amenable to using 'undisturbed' soil samples obtained in the field although natural, disturbed sediments have been used.

4.2.6.4 In-Situ Methods

In light of the many factors affecting the erodibility of cohesive soils there is a strong case to be made for the use of in-situ testing methods. When soils are tested in-situ there is no error associated with extrapolating laboratory results to natural conditions. All physical, chemical and biological factors are as they exist in nature and there is no need for reconstructing soils for testing. A vast majority of in-situ testing methods reported in the literature are for estuarial applications (e.g. Gust and Morris 1989, Houwing and van Rijn 1995, and Ravens and Gschwend 1999). Researchers concerned with riverine and reservoir environments have not been as aggressive in developing this type of technology. Many of the devices mentioned below are developed for salt water applications that can be used or adapted for fresh water environments. A particular benefit would be the use of these devices in reservoirs that often consist of fluid mud that is much more difficult to duplicate in the lab.

The Seaflume system originally developed by Young and Southard (1978) has been modified by Gust and Morris (1989). This system is intended for salt water applications and can be deployed in depths up to 13,123 ft. (4000 m). The tripod structure is built from non-anodized aluminum having a base length of 11.5 ft. (3.5 m) and a height of 9.8 ft (3.0 m). Seaflume utilizes a straight flume 6.4 ft long by 1.4 ft wide by 0.64 ft high (1.95 m × 0.435 m × 0.195 m). The cross section is an inverted U-shape. The side walls of the flume cut approximately 2 in. (5 cm) into the sediment during deployment. Flow through the flume is controlled through a suction pump at the outlet. Velocity through the flume is measured by hot-wire sensors with a frequency response capable of resolving turbulent eddies. Shear stress is measured by epoxy-coated, flush mounted nickel grids. Differential signals from optical sensors positioned at the inlet and outlet are used to calculate instantaneous suspended sediment concentration. Data is stored on a digital cassette for evaluation upon recovery of the system. Output from Seaflume may consist of erosion rate versus time plots, erosion rate versus shear stress (log-log), inlet and outlet concentrations versus time, friction velocity versus time, and photographs of erosion within the flume.

A more portable device was built by Ravens and Gschwend (1999). This flume is 7.9 ft. (2.4 m) in length with a 3.3 ft. long (1.0 m) and consists of only the flume and the hose. The inlet section contains a sand coated, Plexiglas bottom. This inlet section allows the development of the boundary layer before the flow reaches the 3.9 ft (1.2 m) erosion section, which is open to the bed and has a laboratory tested uniform bottom stress. The outlet section of the flume has a 10.6 in. (27 cm) long floor protecting that portion of the bed from erosion due to the turbulence generated at the exit. The cross section is rectangular with a width of 4.7 in. (12 cm) and a height of 2.4 in. (6.0 cm). A mesh grid with 0.4 in. (1.0 cm) openings prevents large objects from entering the flume. A wide base running the length of the flume prevents the apparatus from sinking into the mud and two pieces of angle iron are mounted laterally to the bottom, which stabilizes the flume during operation. Water is pulled through the flume with a shipboard pump. Flow is monitored with a flow meter and a turbidimeter monitors the sediment suspension. Applied shear stress in

the flume is based on a relationship between cross sectionally averaged velocity, shear stress and the Darcy-Weisbach friction factor. With a friction factor obtained from the Moody diagram (Moody, 1944), a power law fit was derived for the applied shear stress over a range of flow rates. Results obtained with this flume are discussed later in this chapter.

The development of a vertically deployed racetrack style flume is reported by Houwing and van Rijn (1995). The flume is 5.9 ft. (1.8 m) long and 2.3 ft. (0.7 m) in overall height. Flow is generated in the top section of the flume by a propeller, which is controlled by an adjustable oil pressure system. The lower portion of the flume is the test section where an open bottom exposes the flow to the bed. The test section has a rectangular cross section with a height of 3.9 in. (0.1 m) and a width of 7.9 in. (0.2 m). Flow is measured by means of an electro-magnetic flow meter and an optical sensor measures suspended sediment. Shear stress was determined from the velocity profile in the laboratory and an equation was derived so that velocity 1.0 in. (2.5 cm) above the bed is all that needs to be measured to obtain an applied shear stress.

As with any experiment, reproducibility is critical for dependable results. Spatial variations in bed topography, composition, and structure can be responsible for widely varied values of critical shear stress for erosion. This further mandates precise testing methods and devices so that variations in results can be attributed to bed variations and not the precision of the instrument.

Cornelisse et al. (1994) have published comparisons of several in-situ and lab erosion testing devices. These investigators concluded that reproducibility improves with an increased surface area.

4.2.7 Critical Shear Stress and Erosion Rate Formulae

This section covers erosion formulae commonly used for critical shear stress and erosion rates. Because there is no comprehensive theory regarding the erosion of cohesive soils the equations presented are empirical. The subsequent sections discuss the applicability of the following equations and how to determine the site specific parameters required for their use.

A formula for the surface erosion rate was presented by Ariathurai (1974) by fitting the experimental plots of erosion rate versus applied shear stress by Partheniades (1962):

$$Q_{se} = \begin{cases} M_{se}\dfrac{\tau - \tau_{se}^{c}}{\tau_{se}^{c}}, & \tau \geq \tau_{se}^{c} \\ 0, & \tau < \tau_{se}^{c} \end{cases} \tag{4.15}$$

where Q_{se} = surface erosion rate,

τ and τ_{se}^{c} = bed shear stress and critical surface erosion shear stress, respectively, and

M_{se} = surface erosion rate constant.

The excess bed shear stress, defined as $\tau - \tau_{se}^{c}$, is a measure of the erosion force. The critical erosion shear stress depends on a number of factors including sediment composition, bed structure, chemical compositions of the pore and eroding fluids, deposition history, and the organic matter and its state of oxidation (Ariathurai and Krone, 1976; Mehta et al., 1989). Usually, both M_{se} and τ_{se}^{c} change with the bed properties in depth and time. Field studies or laboratory measurements must be made to obtain the critical shear stress and the erosion rate.

Hwang and Mehta (1989) presented a relationship with the critical shear stress for surface erosion and the wet bulk density of the bed,

$$\tau_{se}^{c} = a_{se}(\rho_{wb} - \rho_{l})^{b_{se}} + c_{se} \tag{4.16}$$

with a_{se}, b_{se}, c_{se}, and ρ_{l} having default values of 0.883, 0.2, 0.05 and 1.065, respectively for the stress in N/m^2 and the bed bulk density in g/cm^3. They are determined from field data. Hwang and Mehta (1989) also presented a relationship for the erosion constant as a function of the wet bulk density of the bed:

$$\log_{10} M_{se} = 0.23\exp\left(\frac{0.198}{\rho_{wb} - 1.0023}\right) \tag{4.17a}$$

where ρ_{wb} = wet bulk density of the deposit in g/cm^3, and
M_{se} = surface erosion rate constant in mg/cm^2/hr.

According to Teisson and Latteux (1986) and Cormault (1971) the experimental formulation of M_{se} for the Gironde Estuary is:

$$M_{se} = 0.55\left(\frac{\rho_{b}}{1000}\right)^{3} \tag{4.17b}$$

where ρ_{b} = the dry bulk density of the deposit in g/l, and
M_{se} = surface erosion rate in kg/m^2/s.

In the numerical model of Nicholson and O'Connor (1986), the critical erosive stress is assumed to depend on the bed density:

$$\tau_{se}^{c} = \tau_{ef} + A(\rho_{b} - \rho_{f})^{B} \tag{4.17c}$$

where τ_{ef} = critical shear stress of a freshly deposited bed,
ρ_{b}, ρ_{f} = dry bulk density of bed and freshly deposited bed, respectively, and
A and B = constants.

The parameters used in their model are shown in Table 4.4.

Table 4.4. Model erosion parameters

Erosion parameter	Value
τ_{ef}	0.8×10^{-1} N/m^2
ρ_f	80 kg/m^3
A	0.5×10^{-3} N m$^{5/2}$/kg$^{3/2}$
B	1.5

The rate of mass erosion over a time interval Δt is given by (Shrestha and Orlob, 1996)

$$Q_{me} = \frac{T}{\Delta t}\rho_s\left(\frac{\rho_b - \rho_w}{\rho_s - \rho_w}\right) \tag{4.18}$$

where T = thickness of the erodible layer, which is also a function of the excess bed shear stress,
Q_{me} = Mass erosion rate, and
ρ_s, ρ_b, ρ_w = density of sediment material, dry bulk density, and density of the suspending medium, respectively.

4.2.8 Discussion of Cohesive Soil Erosion Parameters Determined Through Experiment

Although direct measurement of cohesive soil properties provides the best possible results for determining erosional and depositional parameters, it is not always practical to do so. Monetary and time constraints often dictate available data. When testing of a specific soil is not possible it becomes necessary to make generalizations for modeling or analysis. This must be done with extreme caution and is not recommended for final results. This section presents some cautions regarding such generalizations and will provide a modeler or engineer with bounded values for erosion parameters, specifically the critical shear stress for particle erosion and ensuing erosion rates. These values vary by many orders of magnitude depending on the various soil parameters mentioned previously in this chapter, however in most cases some information is available about the soil and eroding fluid so that the values can be narrowed to arrive at a reasonable assumption.

Many studies have been performed linking mechanical soil properties to erosional properties, some of which are reviewed below. This has been done in an attempt to link erosion parameters of cohesive soils to some mechanical property. To date this has not been successfully accomplished due to the wide variation of parameters that determine the erodibility of cohesive soils. Smerdon and Beasley (1959) correlated critical shear stress for erosion with the plasticity index (PI), defined as the liquid limit (LL) minus the plastic limit (PL). These values are determined by the Atterberg limits test (Atterberg, 1911). Despite some scatter in the data (regression coefficient, R^2 = 0.77) this study showed an increase in resistance to erosion with

increasing PI. Some investigators have since made similar correlations (Kamphuis and Hall, 1983 and Vermeyen, 1995) without being able to make generalizations about all cohesive soils.

Kamphuis and Hall (1983) made correlations of critical shear stress to unconfined compressive strength and vane shear strength. In this study critical shear stress was plotted with unconfined compressive strength and a regression with an R^2 value of 0.967 was obtained for 10 data points. This good fit of the data is likely due to critical shear stress being determined visually when pits began to appear in the soil sample. By definition this is mass erosion and this failure mechanism is more closely related to the soil's yield strength than is particle erosion. This observation was not reported in the literature. The investigators reported critical shear stress values in the range of 9 to 18 Pascals (Pa), much higher than those determined by other investigators for surface erosion. These values are another indication that critical shear stress for mass erosion was determined. Although a good correlation was obtained for critical shear stress and unconfined compressive strength these values can not be interpreted as applicable to any other soil types. Kamphuis and Hall (1983) arrived at this same conclusion.

Zreik et al. (1998) used a rotating annular flume to determine erosion properties for surface erosion using Boston blue clay. Critical shear stresses with depth were compared with undrained shear strength determined with a fall cone device. Their results show a one order of magnitude difference between the mechanical strength and the erosional strength (approximately 10 to 35 Pa and 0.1 to 1 Pa, respectively).

Although mechanical properties are not transferable from one soil type to another, they are consistent in showing that resistance to erosion is directly proportional to the soil's mechanical strength. It is worthwhile to mention that Partheniades (1965) determined that failure by shear stress applied by flowing water is different from failure by mechanical shear stress applied through the mass of the soil and that the Atterberg limits and mechanical composition can not be used as unique criteria for determining soil erodibility. The findings by Kamphuis and Hall (1983) and Zreik et al. (1998) support this.

4.2.9 Published Results of Erosion Parameters

Studies have been performed to relate erosion of cohesive soils with bulk density (Hwang and Mehta, 1989; Teisson and Latteux, 1986; van Rijn, 1993; Roberts et al., 1998; and others). Roberts et al. (1998) state that the bulk density alone could not be used to determine critical shear stress for erosion and erosion rates, however Hwang and Mehta (1989) were able to obtain expressions to determine the critical shear stress and erosion rate based on bulk density using data from a study performed with sediment from Lake Okeechobee. Because bulk properties are standard and easily determined it would be useful if erosion properties could be linked to bulk properties, however important factors such as sediment composition, salinity and other physico-chemical properties are not taken into account for this type of analysis. An interesting finding by Roberts et al. (1998) is that the erosion rates for sediment sizes greater than 0.125 mm (fine sand) is independent of bulk density, making bulk density a specific parameter for the erosion of cohesive soils. In spite of the shortcomings of determining erosion parameters with bulk density

this may be the best generalization available. Mehta et al (1989) report that density provides an approximate indication of the erosional strength of the bed.

Hwang and Mehta (1989) performed erosion experiments to determine the critical shear stress and the erosion rate for surface and mass erosion using an annular flume with sediment and eroding fluid from Lake Okeechobee, Florida. By obtaining erosion rates and critical shear stress values for various wet bulk densities (ρ_{wb}) they developed Equations (4.16) and (4.17a) for surface erosion and the following relationships for mass erosion:

$$\tau_{me}^{c} = a_{me}\rho_{wb} + b_{me} \tag{4.19}$$

$$M_{me} = const. \tag{4.20}$$

where τ_{me}^{c} = the critical shear stress for mass erosion, in N/m^2,
M_{me} = the erosion rate constant for mass erosion, and
a_{me} and b_{me} = experimentally determined constants (9.808 and –9.934, respectively).

The constant value determined for the mass erosion rate is 224 mg/cm^2 hr. Using Equations (4.16), (4.17a), (4.19), and (4.20), Hwang and Mehta (1989) were able to apply a vertical sediment transport model for various bed depths with profiles of known bulk density. Changes in the concentration profile and bed elevation with time were the output for this model.

Van Rijn (1993) compiled data relating critical shear stress to dry bulk density and reports the following equation:

$$\tau_{se}^{c} = j(\rho_b)^k \tag{4.21}$$

where ρ_b = dry bulk density of the soil in kg/m^3,
τ_{se}^{c} = critical surface erosion shear stress in units of N/m^2, and
j and k = coefficients determined by experiment.

The coefficient k was found to be in the range of 1 to 2.5 (van Rijn, 1993). Thorn and Parsons (1980) found k = 2.3 for mud from the Brisbane River, Australia, Grangemouth Estuary, Scotland and Belawan, Indonesia. Burt (1990) determined that k = 1.5 for mud from Cardiff Bay, England. Van Rijn makes no mention of any values for j in the literature. Re-evaluation of the data to obtain values for j would yield a large range of values due to the wide variation in k. Table 4.5 provides shear strength data from van Rijn (1993) and others related to the dry bulk density.

Table 4.6 provides erosion properties obtained by several investigators using various soils and testing methods. This table can be used as a guide to compare the results from various erosion experiments. Although there is a wide range of values in Table 4.6, erosion properties can be

narrowed according to the soil type and eroding fluid. There is an exhaustive amount of literature providing erosion properties, however the data required to build such a table are not always presented in the literature. The data in Table 4.6 were re-analyzed to obtain the erosion rate parameters, with the exception of those shown for the study by Ravisangar et al. (2001), who published these values in the literature.

Table 4.5. Critical bed shear stress for surface erosion for different dry bulk densities (after van Rijn, 1993)

Soil Type	Sand	Organic	τ_{se}^{c} = critical shear stress for surface erosion [Pa]				
	[%]	[%]	ρ_b =100 [kg/m3]	ρ_b =150 [kg/m3]	ρ_b =200 [kg/m3]	ρ_b =250 [kg/m3]	ρ_b =300 [kg/m3]
Kaolinite (saline water)	0	0	-	0.05 – 0.10	0.30 – 0.40	-	-
Kaolinite (distilled water)	0	0	-	0.05 – 0.10	0.15 – 0.20	0.20 – 0.25	0.25 – 0.30
Hollands Diep 1 (lake)	9	10	0.15 – 0.25	0.30 – 0.40	0.40 – 0.50	0.60 – 0.80	-
Hollands Diep 2 (lake)	23	9	0.15 – 0.25	0.30 – 0.40	0.40 – 0.50	0.80 – 1.00	-
Ketelmeer (lake)	7	12	0.10 – 0.20	0.20 – 0.25	0.25 – 0.35	0.50 – 0.70	-
Biesbosch (lake)	8	8	0.20 – 0.25	0.25 – 0.30	0.30 – 0.35	0.50 – 0.70	-
Maas (river)	36	8	0.15 – 0.30	0.30 – 0.40	0.40 – 0.50	0.80 – 1.00	-
Breskens Harbour (estuary)	27	5	0.15 – 0.25	0.25 – 0.35	0.35 – 0.45	0.60 – 0.80	-
Delfzijl Harbour (estuary)	60	2	0.05 – 0.15	0.15 – 0.20	0.20 – 0.25	0.40 – 0.60	-
Loswal Noord (sea)	69	2	0.20 – 0.30	0.30 – 0.35	0.35 – 0.45	0.60 – 0.80	-
Brisbane, Grangemouth and Belawan	0	-	0.20 – 0.30	0.40 – 0.60	0.80 – 1.00	-	-
Loire	-	-	0.10 – 0.15	0.15 – 0.20	0.20 – 0.30	0.30 – 0.40	0.80 – 1.20
Cardiff Bay	-	-	0.20 – 0.30	0.40 – 0.50	0.60 – 0.70	0.70 – 0.90	-

Table 4.6. Erosion properties determined by several investigators using various methods and soil types

Investigator	Soil type	Flume type	Varied parameter	τ^{c}_{se} [Pa]	τ [Pa]	Q_{se} [kg/m^{2}s]	M_{se} [kg/m^{2}s]	$M_{se,ex}$ [kg/m^{2}s]	a [-]
(1)	(2)	(3)	(4)	(5)	(6)	(7)	(8)	(9)	(10)
Arulanandan et al. (1975)[a]	Yolo loam @ 0.1N salt concentration	Rotating cylinder	Sodium Adsorption Ratio SAR = (12.4)	0.5	0.7 - 1.9	1.8×10^{-3} - 14×10^{-3}	0.0054	-------	----- --
			SAR = (9.4)	1.3	1.6 - 3.6	0.7×10^{-3} - 3.8×10^{-3}	0.0020	-------	-----
			SAR = (1.4)	3.8	5.6 - 6.7	0.9×10^{-3} - 2.5×10^{-3}	0.0055	-------	-----
		Rotating cylinder	SAR = (10.7)	0.05	0.4 - 1.2	5.0×10^{-3} - 15×10^{-3}	0.0009	-------	-----
			SAR = (3.0)	0.2	0.5 - 1.3	3.3×10^{-3} - 8.3×10^{-3}	0.0010	-------	-----
			SAR = (1.6)	0.5	1.0 - 2.1	1.2×10^{-3} - 3.5×10^{-3}	0.0015	-------	-----
Ariathurai and Arulanandan (1978)[a]	30% Illite (remaining material not provided in text)	Rotating cylinder	Temperature = (42°C)	1.2	1.3 - 2.4	0.4×10^{-3} - 4.0×10^{-3}	0.0040	-------	-----
			(23°C)	2.2	2.6 - 4.8	0.5×10^{-3} - 2.8×10^{-3}	0.0023	-------	-----
			(18°C)	2.4	2.6 - 6.0	0.2×10^{-3} - 2.8×10^{-3}	0.0019	-------	-----
			(9.5°C)	2.6	2.6 - 6.0	0.03×10^{-3} - 1.6×10^{-3}	0.0012	-------	-----
Partheniades (1965)[b]	S. F. Bay mud in water at ocean salinity	Straight flume	Placed bed	0.057	.011 - 0.93	0.15×10^{-6} - 5.0×10^{-6}	1.3×10^{-7}	-------	-----
			Flocculated bed	0.057	0.15 - 0.44	0.12×10^{-6} - 1.5×10^{-6}	2.7×10^{-7}	-------	-----
Nachtergale and Poesen (2002)[a,c]	Loess - undisturbed cylinder samples from crop land tested in fresh water	Straight flume	A Horizon	0.57	1.65 - 3.96	1.9×10^{-2} - 15×10^{-2}	0.0299	-------	-----
			B Horizon	0.66	1.65 - 3.96	3×10^{-2} - 4×10^{-2}	f	-------	-----
			C Horizon	1.65	1.65 - 3.96	1×10^{-2} - 41×10^{-2}	0.2827	-------	-----
Dennet et al. (1998)[a]	Kaolinite flocculated bed in fresh water	Straight flume	Natural Organic Matter (NOM) = 0.00%	0.77	0.96 - 1.82	3.7×10^{-3} - 22×10^{-3}	0.0155	-------	----- --
			NOM = 0.002%	0.54	0.97 - 1.67	9.4×10^{-3} - 26×10^{-3}	0.0127	-------	-----
			NOM = 0.006%	0.39	0.97 - 1.67	18×10^{-3} - 40×10^{-3}	0.0121	-------	-----
			NOM = 0.012%	0.36	0.97 - 1.67	19×10^{-3} - 37×10^{-3}	0.0107	-------	-----

Table 4.6. Erosion properties determined by several investigators using various methods and soil types

Investigator	Soil type	Flume type	Varied parameter	τ^c_{se} [Pa]	τ [Pa]	Q_{se} [kg/m^{2}s]	M_{se} [kg/m^{2}s]	$M_{se,ex}$ [kg/m^{2}s]	a [-]
(1)	(2)	(3)	(4)	(5)	(6)	(7)	(8)	(9)	(10)
Ravisangar et al. (2001)[a]	Kaolinite flocculated bed in fresh water	Straight flume	pH of pore and eroding fluid = 3.5	0.91	0.97 - 1.67	1.3×10^{-3} - 12×10^{-3}	0.0151	-------	-------
			pH = 4.0	0.91	0.97 - 1.67	1.9×10^{-3} - 16×10^{-3}	0.0186	-------	-------
			pH = 5.0	0.88	0.97 - 1.67	5.5×10^{-3} - 30×10^{-3}	0.0279	-------	-------
			pH = 6.0	0.12	0.97 - 1.67	14×10^{-3} - 25×10^{-3}	0.0021	-------	-------
			pH = 7.0	-----	0.97 - 1.5	6.0×10^{-3} - 9.2×10^{-3}	f	-------	-------
			pH = 8.0	-----	0.97 - 1.5	2.8×10^{-3} - 3.9×10^{-3}	f	-------	-------
Westrich et al. (1997)	Undisturbed reservoir mud in fresh water	Straight flume	Upper-most horizon	0.74	0.77 - 1.76	0.16×10^{-4} - 4.0×10^{-4}	0.00031	-------	-------
			Second horizon	0.66	0.69 - 1.68	0.77×10^{-4} - 14.4×10^{-4}	0.00087	-------	-------
Johansen et al. (1997)[d,e]	Reconstructed bay (Wadden Sea) mud in water at ocean salinity	Annular flume	Consolidation time = 12 hrs, depth = 0-0.75 cm	0.055-0.20	0.088 - 0.25	7.9×10^{-6} - 64×10^{-6}	-------	0.6776[g]	3.1891[g]
			Consolidation time = 24 hrs, depth = 0-0.81 cm	0.055 - 0.25	0.088 - 0.31	4.6×10^{-6} - 53×10^{-6}	-------	0.3753[g]	3.1415[g]
			Consolidation time = 48 hrs, depth = 0-0.29 cm	0.084 - 0.37	0.11 - 0.44	1.6×10^{-6} - 44×10^{-6}	-------	2.8612[g]	4.1504[g]
Ravens and Gschwend (1999)[a,g]	Boston Harbor mud, in-situ test, 12% clay, 51% silt, saline environment	In-situ flume	Applied shear stress	0.12	0.15-0.49	0.13×10^{-3} - 1.3×10^{-3}	-------	0.0032	1

a. τ^c_{se} was determined with x-intercept of shear stress vs. E curve.

b. Both initial and final erosion rates were reported in the literature however only final erosion rates are reported in this table.

c. Five soil horizons were tested using soil sampled with cylinders from agricultural lands, only results from the top horizon are reported in this table.

d. Applied shear stresses are not reported and are calculated from a best-fit equation and averaged over the three runs.

e. Critical shear stress calculated for several depths.

f. Erosion rate constant, *M* is indeterminate because the slope is near or less than 0.

g. A dimensionless form was not possible, shear stress values must be in Pa (N/m^2).

Many investigations indicate that erosion rates are linear with increasing applied shear stress and can be described by Equation (4.15). Erosion rates for soils exhibiting this property can be determined with the knowledge of the critical shear stress $\left(\tau_{se}^{c}\right)$, applied shear stress (τ), and an erosion rate constant, (M_{se}) shown in columns five, six and eight of Table 4.6. Because the shear stress term is dimensionless the constant will have units associated with it, in this case the units are in [kg/m^{2}s]. This value is obtained by plotting the dimensionless parameter $\left(\frac{\tau}{\tau_{se}^{c}}-1\right)$ against the erosion rate, Q_{se} (Table 4.6, column seven) to find the slope of the line for the value M_{se}.

The erosion rate constant will have the same units as the plotted erosion rate. The applicability of the erosion rates shown in column seven is limited to surface (or particle) erosion. Van Rijn (1993) reports values for M_{se} in the range of 0.00001 to 0.0005 although Table 4.6 shows a much wider variation (0.00000013 to 0.2827), noting that the greatest value for M_{se} is obtained from loess taken from cropland. It is important to note that Equation (4.15) assumes a constant critical shear stress with depth, making it necessary to obtain multiple erosion rate constants for stratified soils. This has been demonstrated in Table 4.6 for experiments performed by Nachtergaele and Poesen (2002) and Westrich et al. (1997).

Soil stratification occurs in heterogeneous soils due to differential settling and depositional history. Deposited soils undergo self weight consolidation, whereby overburden stress causes the soil matrix to collapse, expelling the interstitial fluid and resulting in a decreased void space (Teisson et al., 1993). Decreasing the void space creates a stronger soil matrix due to increased surface contact of the particles. Consolidation will result in greater bed shear strength with depth and is generally related to age unless some mechanical method of compaction is used in laboratory situations. The strengthening of a soil mass with depth is finite and a maximum bed strength will develop that will remain mostly constant, assuming homogeneous soil composition.

The depth at which the bulk density and/or mechanical strength becomes relatively constant appears to occur several centimeters below the sediment surface (Figure 4.4) This gradient may be significant in flume studies or estuaries when cyclic stresses related to tides suspend and redeposit bottom sediment; however, the strength gradient near the soil surface is of little relevance in applications related to erosion in river channels or when deconstructing reservoirs when very little deposition occurs and erosion processes dominate. An assumption of a constant erosion rate with depth is generally acceptable in these situations for homogeneous soils.

Some analyses relate excess shear stress $\left(\tau-\tau_{se}^{c}\right)$ to the erosion rate, as shown in Equation (4.22), where the subscript *se,ex* indicates surface erosion rate determined with excess shear stress. The erosion rate for this type of analysis requires the erosion rate constant ($M_{se,ex}$) to have units of kg/m^{2}sPa (e.g., Ravens and Gschwend, 1999 in Table 4.6). This analysis is very similar to Equation (4.15), the difference being that Equation (4.22) does not have a dimensionless shear stress term. If a soil exhibits exponential surface erosion rates with increasing shear stress, the α

term will have a value other than one. For example, the study by Johansen et al. (1997) reports exponential erosion rates conforming to Equation (4.22) with an α value > 1. The constants for an exponential relationship are shown in columns nine and ten of Table 4.6, where $M_{se,ex}$ is an erosion rate constant associated with a dimensional excess shear stress and α is the exponent, both determined by a best fit equation of excess shear stress $\left(\tau - \tau_{se}^{c}\right)$ plotted against the erosion rate (Q_{se}).

$$Q_{se} = M_{se,ex}\left(\tau - \tau_{se}^{c}\right)^{\alpha} \tag{4.22}$$

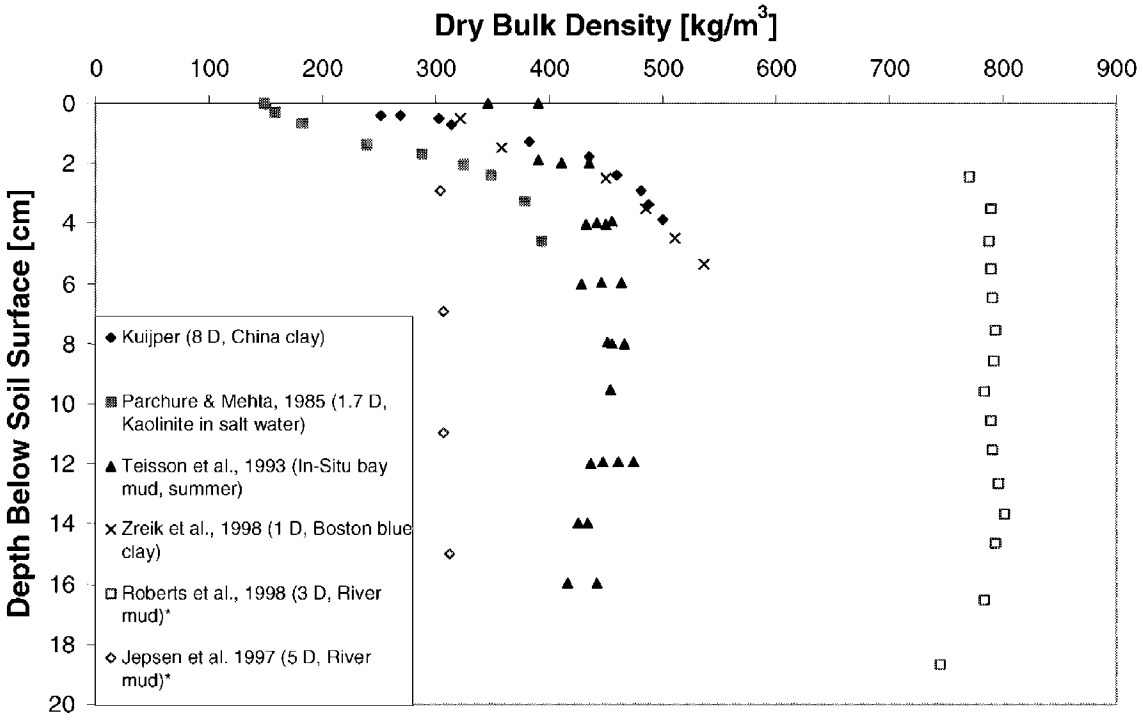

Figure 4.4. Chart comparing various bulk densities with depth. Ages of reconstructed soils range from 1.7 days (D) to 8 days. *Dry density obtained from reported wet bulk density by subtracting 1000 kg/m^3.

An equation taking the form of Equation (4.22) does not provide a dimensionless shear stress term, making it necessary to use units of Pa (N/m^2) for applied (τ) and critical $\left(\tau_{se}^{c}\right)$ shear stress if the erosion rate constant shown in column nine of Table 4.6 is to be used to obtain a rate in [kg/m^{2}s]. It is possible that an equation such as Equation (4.22) could represent both surface and mass erosion with mass erosion occurring soon after the break in slope on the graph, however, this has not been demonstrated in the literature.

For testing the upper portion of an estuarial sediment bed, Parchure and Mehta (1985) found that the methods described above were not applicable for the very soft, partially consolidated soils found in the upper few centimeters of the bed. These investigators incorporated the rate process

theory to describe the time dependent particulate deformation of soft cohesive soils, which is applicable to soils exhibiting varying strength with depth (unlike Equation 4.15). This method uses the threshold energy concept to describe an erosion rate based on the excess shear stress $\left(\tau - \tau_{se}^{c}\right)$ and $\ln(Q_{se})$ (Kelly and Gularte, 1981). The resulting equation is shown below (Parchure and Mehta, 1985):

$$\ln \frac{Q_{se}}{Q_f} = \beta\left(\tau - \tau_{se}^{c}\right)^{1/2} \tag{4.23}$$

where Q_f = Q_{se} when $\tau = \tau_{se}^{c}$, defined as the point at which no velocity dependent surface erosion occurs, and

β = a factor inversely proportional to temperature.

Use of this equation assumes the knowledge of the increase in erosional strength with depth. Floc erosion Q_f occurs in spite of the fact that $\tau = \tau_{se}^{c}$ because there is some entrainment due to the stochastic nature of these parameters. Determining Q_f experimentally can be very time intensive and may be alternately obtained when the $\ln(Q_{se})$ is plotted against $\left(\tau - \tau_{se}^{c}\right)^{1/2}$, where Q_f is the intercept of the $\ln(Q_{se})$ axis (Parchure and Mehta, 1985). Values of β and Q_f obtained by several authors are contained in Table 4.7.

Table 4.7. Erosion rate parameters used in Equation (4.23) (After Parchure and Mehta, 1985 with additional data from Kuijper et al., 1989 and Winterwerp et al., 1993)

Investigator	Soil Type	β ($m/N^{1/2}$)	$Q_f \times 10^6$ (kg/m^2s)
Parchure and Mehta (1985)	Kaolinite in tap water	18.4	0.83
	Kaolinite in salt water	17.2	2.3
	Lake mud	13.6	5.3
Partheniades (1965)	Bay mud	8.3	0.067
Lee (1979)	Lake mud	8.3	0.7
Thorn and Parsons (1977)	Estuarial mud	8.3	0.7
Thorn and Parsons (1979)	Estuarial mud	4.2	3.1
Dixit (1982)	Kaolinite	25.6	1.0
Kuijper et al. (1989)	China clay in annular flume	12 - 28	0.3 – 3.3
	China clay in tidal flume	27	0.2 – 1.1
Winterwerp et al. (1993)	Harbor mud	10	0.5

The laboratory use of Equation (4.23) appears to be limited to annular flumes, with soft deposited beds. This set-up best represents estuarial situations where cyclic conditions related to tides dominate the erosion process, where a soft fluid mud layer exists at the sediment-water interface.

For this type of application sediment is deposited, resuspended and deposited again, without ample time for complete consolidation. The top several centimeters of the soil are critical, as this is generally the extent of the erosion (over shorter time periods, e.g. days). For this situation an increase in bed shear strength with depth is significant, as opposed to riverine applications where a bed may be expected to undergo only erosion of a consolidated bed.

Most applications related to erosion of cohesive soils involve surface erosion, which has been the focus of the preceding discussion. When mass erosion occurs it is generally indicated on a graph by a break in slope, so that the erosion rate is shown to increase (see Figure 4.3). A separate critical shear stress (τ_{me}^{c}) and erosion rate constant (M_{me}) would be necessary for mass erosion and can be plotted on the same graph.

4.3 Numerical Models of Cohesive Sediment Transport

Numerical models are becoming a useful tool to predict cohesive sediment transport. Numerical models solve the mass transport equation for suspended sediment and the mass conservation equation for bed sediment after the hydraulic field is solved. In the following, numerical models are reviewed based on the number of dimensions of the model. Chapter 5 emphasizes non-cohesive sediment transport numerical models.

4.3.1 One-Dimensional Models

One-dimensional models solve the unsteady, cross-sectionally averaged equation for the mass balance of suspended sediment:

$$\frac{\partial(Ac_i)}{\partial t}+\frac{\partial(Qc_i)}{\partial x}=\frac{\partial}{\partial x}(AD_x\frac{\partial c_i}{\partial x})+S_i \tag{4.24}$$

where A = cross-sectional area (m^2),
Q = discharge (m^3/s),
c_i = cross-sectionally averaged sediment volume concentration (m^3/m^3) of constituent i,
t = time,
u = cross-sectionally averaged velocity components (m/s) in the streamwise direction x,
D_x = dispersion coefficient (m^2/s) in the streamwise direction x, and
S_i = source (erosion) and sink (deposition) terms (m^2/s) for constituent i.

Most 1D models are mainly designed for non-cohesive sediment transport with the capacities to simulate simple processes of cohesive sediment transport. These models include HEC-6 (U.S. Army Corps of Engineers, 1993), GSTARS 2.1, and GSTARS3 (Yang and Simões, 2000, 2002) and GSTAR-1D (Yang et al., 2004, 2005).

EFDC1D (Hamrick 2001) is a 1D sediment transport model that includes settling, deposition and resuspension of multiple size classes of cohesive and non-cohesive sediments. A bed consolidation model is implemented to predict time variations of bed depth, void ratio, bulk density and shear strength. Other contributions to 1D models of cohesive sediment transport were made by Odd and Owen (1972), Scarlatos (1981), and Li and Amos (1995).

4.3.2 Two-Dimensional Models

Two-dimensional models solve the depth-averaged or width-averaged convection-diffusion equation with appropriate boundary conditions. The 2D depth-averaged advection-dispersion equation for cohesive sediment transport is:

$$\frac{\partial(Dc_i)}{\partial t}+\frac{\partial(Duc_i)}{\partial x}+\frac{\partial(Dvc_i)}{\partial y}=\frac{\partial}{\partial x}(D_xD\frac{\partial c_i}{\partial x})+\frac{\partial}{\partial y}(D_yD\frac{\partial c_i}{\partial y})+S_i \qquad (4.25)$$

where D = depth (m),
c_i = depth-averaged concentration (m^3/m^3) of constituent i,
t = time (s),
u, v = depth-averaged velocity components (m/s) in the streamwise and transverse or vertical directions, x and y, respectively,
D_x, D_y = dispersion coefficients (m^2/s) in the x and y directions, respectively, and
S_i = source (erosion) and sink (deposition) terms (m/s) for constituent i.

Usually, three types of boundary conditions are encountered in a 2D numerical model. At the inlet boundary, the sediment concentration is given. At the outlet boundary, there is no concentration gradient. At solid boundaries, there is no horizontal flux normal to the solid surface. Two-dimensional models have been applied to channel sedimentation and harbor sedimentation studies, where the variation of flow parameters with depth or width can be neglected.

SED2D WES (Letter et al., 2000) is a 2D finite element model for cohesive sediment transport developed by the US Army Waterways Experiment Station based on the original works of Ariathurai (1974) and Ariathurai and Krone (1976). Both cohesive and non-cohesive sediment can be simulated, but the model considers a single, effective grain size during each simulation.

Hayter (1983) developed an uncoupled, unsteady, 2D, finite element model for cohesive sediment transport. Further development of this model results in a well-documented numerical model HSCTM-2D (Hayter et al., 1999) with improved algorithm efficiency.

More 2D models were developed for applications to a variety of problems involving channel sedimentation, harbor sedimentation, and delta growth (Onishi, 1981; Cole and Miles, 1983; Teisson and Latteux, 1986 Ziegler and Lick, 1986; Gailani et al., 1991; and Ziegler and Nisbet, 1995; and Shrestha and Orlob, 1996).

4.3.3 Three-Dimensional Models

Three-dimensional (3D) models solve the full convection-diffusion equation, with appropriate boundary conditions. The general equation of transport of cohesive sediment is written:

$$\frac{\partial c_i}{\partial t}+\frac{\partial (uc_i)}{\partial x}+\frac{\partial (vc_i)}{\partial y}+\frac{\partial (wc_i)}{\partial z} = \frac{\partial}{\partial x}(D_x \frac{\partial c_i}{\partial x})+\frac{\partial}{\partial y}(D_y \frac{\partial c_i}{\partial y})+\frac{\partial}{\partial z}(D_z \frac{\partial c_i}{\partial z})+\frac{\partial}{\partial z}(\omega c_i) \tag{4.26}$$

where c_i = volume concentration (m^3/m^3) of sediment constituent i,
t = time (s),
u, v, and w = velocity components (m/s) in the directions, x, y, and z, respectively
D_x, D_y, D_z = dispersion coefficients (m^2/s) in the x, y, and z directions, respectively, and
ω = sediment fall velocity (m/s).

The source and sink terms, i.e., erosion and deposition fluxes, are incorporated in the bed boundary conditions, written as:

$$(D_z \frac{\partial c_i}{\partial z})_B = Q_e - Q_d \tag{4.27}$$

where Q_e and Q_d= volume eroded and deposited per unit area per unit time (m/s), respectively, and the subscript B denotes the boundary condition at the bed.

At the water surface, the upward diffusion rate is equal to the downward settling rate, which yields the water surface boundary condition,

$$\left(D_x \frac{\partial c_i}{\partial z}\right)_s = -\omega c_i \tag{4.28}$$

where subscript s = the boundary condition at water surface.

At solid boundaries, there is no diffusion normal to the solid surface, that is

$$D_m \frac{\partial c_i}{\partial n_m} = 0 \tag{4.29}$$

where n_m = the unit normal vector of the boundary.

Until recently, 3D numerical models were only used in academic areas. They may be the future of engineering models, but there are gaps in applying them for engineering purposes. The

computing time required limits them to relatively short reaches of river for short time durations. Another factor that limits the use of a 3D model is the amount of field data needed for the calibration and verification of the 3D model.

The U.S. Army Corps of Engineers developed a 3D sediment transport model, CH3D-WES, that solves the complete 3D advection-dispersion equation using a finite-difference method (Sheng, 1983). Spasojevic and Holly (1996) generalized the 3D model (Sheng, 1986) to include cohesive-sediment capability. A new conceptual model was designed, in which the cohesive sediment can move in suspension, rest on the bed as settled mud, or occasionally form a layer of fluid mud. The suspended sediment can only be deposited onto the fluid mud, and the bed sediment can only be eroded from the settled mud. A thin active layer was used for erosion modeling. EFDC (Environmental Fluid Dynamics Code, Tetra Tech, Inc., 2000) is another 3D surface water model for hydrodynamic and sediment transport simulations in rivers, lakes and estuaries. The physics of the EFDC model and many aspects of the computational scheme are similar to the U. S. Army Corps of Engineers' 3D code CH3D-WES. Other 3D models were developed and applied by Nicholson and O'Connor, (1986), and Hayter and Pakala (1989).

4.3.4 Numerical Models of Contaminant Transport

Numerical models can also be used to predict the fate of contaminants. Numerical models solve the advection-diffusion equation for contaminants after the hydraulic field and sediment transport is solved. A 2D advection-diffusion equation for contaminates is given in the following as a reference.

Assuming instantaneous local equilibrium and constant partition coefficient between two phases of toxicant, the 2D equation for the total toxicant concentration is written as:

$$\frac{\partial(hc_t)}{\partial t}+\frac{\partial(huc_t)}{\partial x}+\frac{\partial(hvc_t)}{\partial y}=\frac{\partial}{\partial x}(D_x h\frac{\partial c_t}{\partial x})+\frac{\partial}{\partial y}(D_y h\frac{\partial c_t}{\partial y})+S \qquad (4.30)$$

where h = depth (m),
c_t = depth-averaged toxicant volume concentration (m^3/m^3),
t = time (s),
u, v = depth-averaged velocity components (m/s) in the horizontal streamwise and transverse directions, x and y, respectively,
D_x, D_y = dispersion coefficients (m^2/s) in the x and y directions, respectively, and
S = source terms (m/s).

Deposition of suspended sediment removes toxicants from the water column. The source term from deposition can be obtained from Equation (4.13) as

$$S = -\frac{f_p C_t \rho_s}{C_s \rho_c} Q_d = -\frac{f_p c_t}{c_s} Q_d \tag{4.31}$$

where Q_d = the sediment deposition rate (m/s),
C_t, C_s = total toxicant and sediment concentration by weight (kg/m^3),
c_t, c_s = total toxicant and sediment concentration by volume (m^3/m^3),
f_p = the fraction of toxicant in the adsorbed phase, and
ρ_c, ρ_s = dry density (kg/m^3) of toxicant and sediment, respectively.

Erosion of bed sediment brings toxicants into the water column. The source term from sediment erosion can be obtained from Equation (4.14) as

$$S = \frac{f_p C_{t,b} \rho_s}{C_{s,b} \rho_c} Q_e = \frac{f_p c_{t,b}}{c_{s,b}} Q_e \tag{4.32}$$

where Q_e = sediment erosion rate, surface or mass (m/s), and
$c_{t,b}$, $c_{s,b}$ = total toxicant and sediment volume concentration (m^3/m^3) in the bed.

The source term from chemical degradation or decay can be written as:

$$S_{de} = \lambda h c_t \tag{4.33}$$

where λ = chemical degradation rate or radionuclide decay rate (s^{-1}).

Shrestha and Orlob (1996) solved the 2D toxicant transport equation similar to Equation (4.30) to predict the fate of heavy metals in South San Francisco Bay.

There are some other numerical models to solve the toxicant transport. One example is HSCTM-2D (Hayter et al., 1999), which solves separate 2D transport equations for both dissolved and adsorbed toxicants. The equation is more complex, however it takes into account the adsorption of dissolved contaminants and the desorption of adsorbed contaminants onto and from suspended sediments, respectively.

4.4 Numerical Model GSTAR-1D

The first version of GSTARS was developed by Molinas and Yang (1985) to simulate the flow conditions in a semi-two-dimensional manner and the change of channel geometry in a semi-three-dimensional manner. Significant efforts were made to improve the first version and GSTARS 2.1 and GSTARS3 were released by Yang and Simões (2000, 2002).

U.S. EPA (Environmental Protection Agency) and the BOR (Bureau of Reclamation) are funding partners in the development of this numerical model for 1D river simulation. While basic concepts of GSTARS (Yang and Simões, 2000) have been retained, the program has been mostly

rewritten. The numerical model, named GSTAR-1D, solves hydraulic and both cohesive and non-cohesive sediment transport, for steady and unsteady flow problems and for single and interconnected channels.

GSTAR-1D (Yang, et al., 2004, 2005) is a hydraulic and sedimentation numerical model developed to simulate flows in rivers and channels with or without movable boundaries. Some of its features are:

- Computation of water surface profiles in a single channel or multi-channel looped networks
- Steady and unsteady flows
- Subcritical flows in a steady hydraulic simulation
- Subcritical, supercritical, and transcritical flows in an unsteady hydraulic simulation
- Steady and unsteady sediment transport
- Transport of cohesive and non-cohesive sediments
- Cohesive sediment aggregation, deposition, erosion, and consolidation
- Sixteen different non-cohesive sediment transport equations that are applicable to a wide range of hydraulic and sediment conditions
- Cross stream variation in hydraulic roughness
- Exchange of water and sediment between main channel and floodplains
- Fractional sediment transport, bed sorting, and armoring
- Computation of width changes using theories of minimum stream power and other minimizations
- Point and non-point sources of flow and sediments
- Internal boundary conditions, such as time-stage tables, rating curves, weirs, bridges, and radial gates.

4.4.1 Conceptual Model

This section describes the conceptual model to simulate cohesive sediment transport in natural river systems. Figure 4.5 is a diagram of the proposed conceptual model, in which the bed is composed of an active layer and a maximum of N-1 inactive layers. In this figure, h = layer thickness, $P_{n,k}$ = volume fraction of k-th size class in layer n. The proposed model will be able to simulate both non-cohesive and cohesive sediment at the same time. A maximum of nf size fractions will be used to represent the sediment size distributions. The existing model will be modified to include cohesive sediment processes, such as settling, deposition, erosion, and consolidation. Consolidation of the sediment bed will be modeled by discretizing the bed into several layers.

The bed profile is considered to be composed of a number of layers of various thickness and bulk density. In each layer, bulk density of the cohesive sediment increases according to the empirically derived consolidation rate, and the bulk density of the non-cohesive sediment is constant. During consolidation, the bed thickness decreases and no mixing exists between each layer.

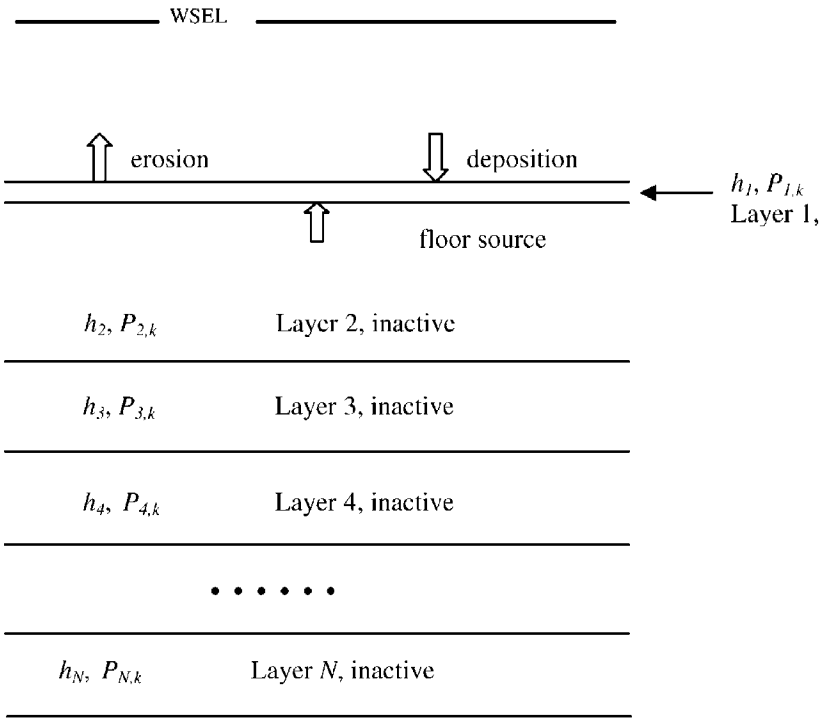

Figure 4.5. Diagram of the conceptual model.

The notion of an active layer provides an appropriate framework for erosion and deposition modeling. The active layer is defined as a thin upper layer of constant thickness. The active layer thickness is defined by the user as proportional to the geometric mean of the largest size class. Uniform size distribution and bulk density are assumed over the active layer depth. It is also assumed that all sediment particles of a given size class inside the active layer are equally exposed to the flow. Convincing experimental evidence shows that the presence of the fine cohesive sediment in the bed can cause the bed's strength to be greater than the shear stress required to entrain individual particles. The model assumes that the erosion rates of silts, sands and gravels are limited to the entrainment rate of the clay when more than 10% of the bed is composed of clay. The notion of an active layer allows the possibility of erosion of only fine sediment on the streambed surface. If the bed-shear stress is larger than the critical shear stress for the finer size classes, but smaller than that for coarser size classes, only the finer size classes are eroded. This will eventually armor the bed surface and prevent further erosion.

The active layer contains the bed material available for transport. During net erosion, the first inactive layer supplies material to the active layer. During net deposition, the additional material is moved to the first inactive layer. A range is set for the thickness of the first inactive layer. The lower limit is set to allow enough sediment to be supplied to the active layer during erosion. The upper limit is set to provide enough accuracy in simulating the bed layer. In the numerical model, the lower and upper limits are set to two and ten times the active layer thickness, respectively.

When the first inactive layer thickness becomes thinner than the lower limit, it merges with the second inactive layer. On the other hand, when it becomes thicker than the upper limit, it is divided into two inactive layers. All the others layer are shifted accordingly.

4.4.2 Active Layer Calculation

The use of an active layer provides a mechanism to model winnowing and armoring. Sediment can only be eroded from or deposited onto the active layer. The active layer thickness is defined by an auxiliary relation to represent the armoring thickness. One can define the thickness as proportional to the geometric mean of the largest size class containing at least 1% of the bed material at that location.

As the bed elevation descends or ascends during erosion or deposition, the active-layer floor changes its elevation to keep the active-layer thickness constant, as shown in Figure 4.6. The movement of the active-layer floor generates the active-layer floor source $S_{f,k}$ for the k-th size class. The kinematic condition of the k-th size fraction can be written as:

$$h_a \frac{dP_{a,k}}{dt} = -\frac{S_{e,k}}{\bar{\varepsilon}_k} + \frac{S_{f,k}}{\tilde{\varepsilon}_k} \tag{4.34}$$

where $P_{a,k}$ = active layer and size class, respectively
$S_{e,k}$ and $S_{f,k}$ = the active layer erosion source and floor source, respectively, and
$\bar{\varepsilon}_k$ and $\tilde{\varepsilon}_k$ = the volume of sediment in a unit bed layer volume (one minus porosity) of the erosion source and the floor source, respectively.

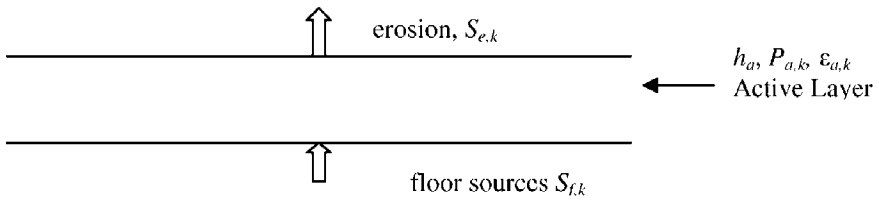

Figure 4.6 Diagram of the active layer model.

During net erosion, $\bar{\varepsilon}_k$ takes the value of the active layer ($\varepsilon_{a,k}$) and $\tilde{\varepsilon}_k$ takes the value of layer 2 ($\varepsilon_{2,k}$). On the other hand, during net deposition, $\bar{\varepsilon}_k$ takes the value of the freshly deposited sediment ($\varepsilon_{i,k}$) and $\tilde{\varepsilon}_k$ takes the value of the active layer ($\varepsilon_{a,k}$). Thus $\bar{\varepsilon}_k$ and $\tilde{\varepsilon}_k$ can be expressed as:

$$\bar{\varepsilon}_k = \begin{cases} \varepsilon_{a,k} & net\ erosion \\ \varepsilon_{i,k} & net\ deposition \end{cases} \tag{4.35}$$

$$\tilde{\varepsilon}_k = \begin{cases} \varepsilon_{2,k} & net\,erosion \\ \varepsilon_{a,k} & net\,deposition \end{cases} \tag{4.36}$$

where the subscript *i* represents freshly deposited sediment and:

$$\varepsilon_{n,k} = 1 - p_{n,k} \tag{4.37}$$

where $p_{n,k}$ = the porosity of the *k*-th size class in layer *n*.

By using the porosity of sediment, one can express the bulk density as:

$$\rho_{n,k} = \rho_s (1 - p_{n,k}) = \varepsilon_{n,k} \rho_s \tag{4.38}$$

where ρ_s = the density of sediment.

Summation of Equation (4.34) with the basic constraint of size fractions $\sum_k P_{n,k} = 1$ gives the global mass-conservation equation for the active layer:

$$\sum_k \frac{S_{e,k}}{\bar{\varepsilon}_k} = \sum_k \frac{S_{f,k}}{\tilde{\varepsilon}_k} \tag{4.39}$$

that shows that the change of the bed elevation due to erosion (or deposition) is the same as the change in the active-layer floor and the active-layer thickness is kept constant.

According to the definition of the volume fraction of a size class, Equation (4.34) can be written as:

$$h_a \frac{dP_{a,k}}{dt} = -\frac{S_{e,k}}{\bar{\varepsilon}_k} + \tilde{P}_k \sum_k \frac{S_{f,k}}{\tilde{\varepsilon}_k} = -\frac{S_{e,k}}{\bar{\varepsilon}_k} + \tilde{P}_k \sum_k \frac{S_{e,k}}{\bar{\varepsilon}_k} \tag{4.40}$$

where $\tilde{P}_k$ can be expressed as:

$$\tilde{P}_k = \begin{cases} P_{2,k} & net\,erosion \\ P_{a,k} & net\,deposition \end{cases} \tag{4.41}$$

where the subscripts *a* and *2* represent the active layer and layer 2, (the first inactive layer) respectively, and the subscript *k* represents the size class.

The mass-conservation equation for *k*-th size class in active layer is:

$$\frac{d}{dt}(\varepsilon_{a,k} P_{a,k} h_a) = -S_{e,k} + S_{f,k} \tag{4.42}$$

By substituting Equation (4.40) into Equation (4.42), one can express the change of $\varepsilon_{a,k}$ as:

$$\frac{d}{dt}\varepsilon_{a,k} = -(1 - \frac{\varepsilon_{a,k}}{\bar{\varepsilon}_k})\frac{S_{e,k}}{P_{a,k} h_a} + (1 - \frac{\varepsilon_{a,k}}{\tilde{\varepsilon}_k})\frac{\tilde{\varepsilon}_k \tilde{P}_k}{P_{a,k} h_a}\sum_k \frac{S_{e,k}}{\bar{\varepsilon}_k} \tag{4.43}$$

Equations (4.40) and (4.43) are essentially the equations for erosion and deposition, respectively, of the active layer.

4.4.3 Consolidation

Consolidation changes the thickness of the bed through changes in porosity. It should be noted that the consolidation process also affects the size-fraction distribution within the bed. Due to the slow rate at which consolidation occurs, the simulation of erosion and deposition are uncoupled from the bed consolidation process. Simulation of bed consolidation should be applied to both the active layer and inactive layers.

During consolidation, the mass of each size fraction remains constant. The mass-conservation equation for the sediment in each layer is:

$$\varepsilon_{n,k} P_{n,k} h_n = Const \tag{4.44}$$

where $P_{n,k}$ = volume fraction of k-th size class in layer n, and
h_n = thickness of layer n.

Equation (4.44) can also be written as:

$$P_{n,k}^{t+\Delta t} h_n^{t+\Delta t} = \varepsilon_{n,k}^{t} P_{n,k}^{t} h_n^{t} / \varepsilon_{n,k}^{t+\Delta t} \tag{4.45}$$

where t = the time step before consolidation, and
$t + \Delta t$ = the time step after consolidation.

Summation of Equation (4.45) with the basic constraint of size fractions $\sum_k P_{n,k} = 1$ gives the global mass conservation equation for sediment in layer n, i.e.:

$$h_n^{t+\Delta t} = \sum_k (\varepsilon_{n,k}^{t} P_{n,k}^{t} h_n^{t} / \varepsilon_{n,k}^{t+\Delta t}) \tag{4.46}$$

Equations (4.45) and (4.46) yield the expression for the size fraction change as:

$$P_{n,k}^{t+\Delta t} = \frac{\varepsilon_{n,k}^{t} P_{n,k}^{t} h_n^t / \varepsilon_{n,k}^{t+\Delta t}}{\sum_k (\varepsilon_{n,k}^{t} P_{n,k}^{t} h_n^t / \varepsilon_{n,k}^{t+\Delta t})} \tag{4.47}$$

Equations (4.46) and (4.47) are essentially equations for bed consolidation.

A similar relationship to the one used in SED2D WES (Letter, et al., 2000) is used here to calculate the change of volume concentration of sediment at bed $\varepsilon_{n,k}$.

$$\varepsilon = \varepsilon_f - (\varepsilon_f - \varepsilon_i) e^{-\beta t} \tag{4.48}$$

where β is the consolidation coefficient computed from user input for initial density as:

$$\beta = \log\left(\frac{\rho_f - \rho_i}{\rho_f - \rho_e}\right) \tag{4.49}$$

where ρ_i = fully consolidated density,
ρ_f = density, and
ρ_e = density at reference time t_e.

So the change of ε can be written as:

$$\frac{d\varepsilon}{dt} = \beta(\varepsilon_f - \varepsilon) \tag{4.50}$$

An explicit Euler scheme is used to calculate the sediment volume in a unit volume after consolidation and is shown here:

$$\varepsilon_{n,k}^{t+\Delta t} = \varepsilon_{n,k}^{t} + d\varepsilon = \varepsilon_{n,k}^{t} + \beta(\varepsilon_f - \varepsilon) dt \tag{4.51}$$

The bed thickness and sediment size fraction can be calculated with Equations (4.46) and (4.47).

4.4.4 Bed Merge

After each time step, the first inactive layer thickness is checked. Once the thickness decreases below the minimum limit, the content of the layer is merged with the underlying layer. The minimum limit of the first inactive layer thickness is set to allow enough sediment supply to the active layer during net erosion. It is obvious that the bed merge is not a physical process, but is a requirement of the discretized representation of the sediment bed.

During the merge of two layers, the new layer thickness is the sum of the two merged layers:

$$h = h_n + h_{n+1} \tag{4.52}$$

and the volume size fraction is:

$$P_k = \frac{P_{n,k} h_n + P_{n+1,k} h_{n+1}}{h_n + h_{n+1}} \tag{4.53}$$

The mass conservation equation is used to obtain ε_k:

$$\varepsilon_k = \frac{\varepsilon_{n,k} P_{n,k} h_n + \varepsilon_{n+1,k} P_{n+1,k} h_{n+1}}{P_k h} \tag{4.54}$$

4.4.5 Example Application

The GSTAR-1D was applied to the California Aqueduct near Arroyo Pasajero to study the influence of rainfall-runoff on sedimentation and water quality (Klumpp, et al., 2003). An unsteady flow and unsteady sediment model was used to simulated a duration of 800 hrs. GSTAR-1D is a numerical model for predicting cohesive and non-cohesive sediment transport, using steady or unsteady flow and can be applied to a simple channel as well as channel networks. The example presented here is not intended to show the readers how to set-up input data files and use GSTAR-1D, however it will provide a general idea of GSTAR-1D's capabilities related to cohesive sediment transport. Interested readers should refer to the GSTAR-1D User's Manual (Yang et al., 2004, 2005) for details on how to use GSTAR-1D.

The studied reach of the California Aqueduct, or San Luis Canal (SLC), extends 75 miles from Check Structure 15 to Check Structure 21. The SLC was designed and built to distribute water for both agricultural and municipal uses. It was built with drain inlet structures to capture floodwaters generated west of the SLC. Rainfall-runoff is admitted to the SLC when the capacity of ponding areas or bypass structures is exceeded. The runoff carries many tons of sediment into the aqueduct. The input data includes the cross-section geometry, the six check structures and their radial gate operations. Main channel flow through the aqueduct was assumed to be 2000 cfs. Six lateral inflows were modeled for the 100 year flood (Table 4.8).

These lateral inflows were modeled in terms of discharge hydrographs and sediment inflows. The bed material along the aqueduct is approximately 2% sand (non-cohesive sediment) and 98% silt and clay (cohesive sediment).

Table 4.8. Lateral inflows used in the GSTAR-1D example

Lateral flow	River mileage (mi)	Maximum discharge (cfs)
Cantua 4 barrel 6 X 4 Drain Inlets	133.67	1,002
Cantua Concrete Flume	134.81	850
Cantua Concrete Weir	134.87	2,743
Salt Creek Drain Inlets	136	112
Salt Creek Drain Inlet metal pipe	137.08	100
Arroyo Pasajero Drain	159	4,500

The present model used a modified version of Equation (4.15) for surface erosion

$$Q_{se} = \begin{cases} P_{se}\left(\dfrac{\tau - \tau_{se}^{c}}{\tau_{me}^{c} - \tau_{se}^{c}}\right) & \tau \geq \tau_{se}^{c} \\ 0 & \tau < \tau_{se}^{c} \end{cases} \tag{4.55}$$

where τ_{me}^{c} = critical mass erosion shear stress.

The modified relationship is more consistent with the mass erosion rate used below. The parameters τ_{se}^{c} and P_{se} are site-specific and have to be determined experimentally. Mass erosion is usually arbitrarily dependent on the model setup and its time scale used. The presented model takes the similar equation for mass erosion as the surface erosion.

$$Q_{me} = P_{me}\left(\frac{\tau - \tau_{me}^{c}}{\tau_{me}^{c}}\right) + P_{se} \qquad \tau \geq \tau_{me}^{c} \tag{4.56}$$

where Q_{me} = mass erosion rate,

τ and τ_{me}^{c} = bed shear stress and critical mass erosion shear stress, respectively, and

P_{me} = mass erosion constant.

Because physical experiments were not able to be performed, observation was used to determine the parameters for cohesive sediment transport. The critical shear stresses for full deposition, partial deposition, surface erosion, and mass erosion were determined from the observations in the channel during various discharges. These parameters are listed in Table 4.9.

Table 4.9. Cohesive sediment parameters for erosion and deposition used in the GSTAR-1D example

Process	Discharge (cfs)	Shear Stress (lb/ft^2)
Full deposition	2,000	0.003
Partial deposition	2,000	0.003
Surface erosion	8,000	0.005
Mass erosion	>>10,000	0.01

The surface erosion rate was calibrated and set to 0.3 $lb/ft^2/hr$.

Eqs. (4.6a-e) are used for cohesive sediment deposition. The settling velocities, due to sediment flocculating, are usually site-specific and need to be determined experimentally. GSTAR-1D allows the user to provide a set of user specified data as shown in Figure 4.7.

The parameters used in the example are listed in Table 4.10.

Table 4.10. Cohesive sediment parameters for fall velocity used in the GSTAR-1D example

Point	*C* (mg/l)	*V* (mm/s)
1	200	0.2
2	6,000	0.2
3	20,000	0.35
4	100,000	0.35

An equilibrium sediment concentration for partial deposition of 265 mg/l was observed at the downstream end of the channel, therefore an equilibrium concentration of 265 mg/l was used in the model.

Figure 4.8 shows the bed elevations before and after the flood. The fine sands allowed into the aqueduct are deposited just downstream of the inlet, raising the channel bed elevation. The fine sands are eroded after the flood, and the bed geometry returns to its initial form after the flood.

Figure 4.9 shows concentration changes with the sediment inflow from the Cantua Creek four barrel drain inlet. The peak sediment inflow concentration from Cantua Creek is about 7,500 mg/l. The peak concentration downstream of the inlets is about 2,000 mg/l. The baseline conditions prior to the lateral sediment inflow is 200 mg/l.

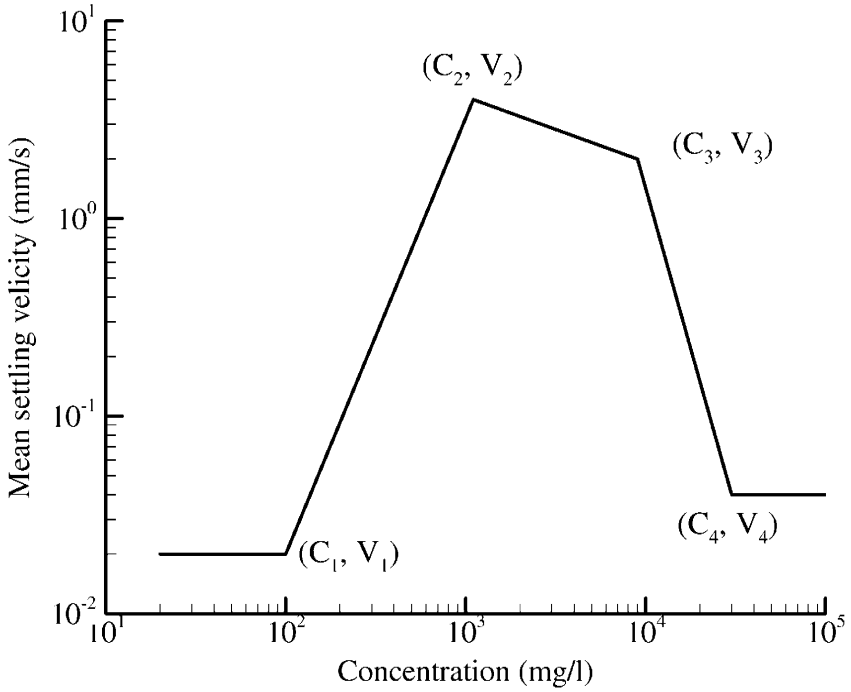

Figure 4.7. Input data illustration for settling velocity

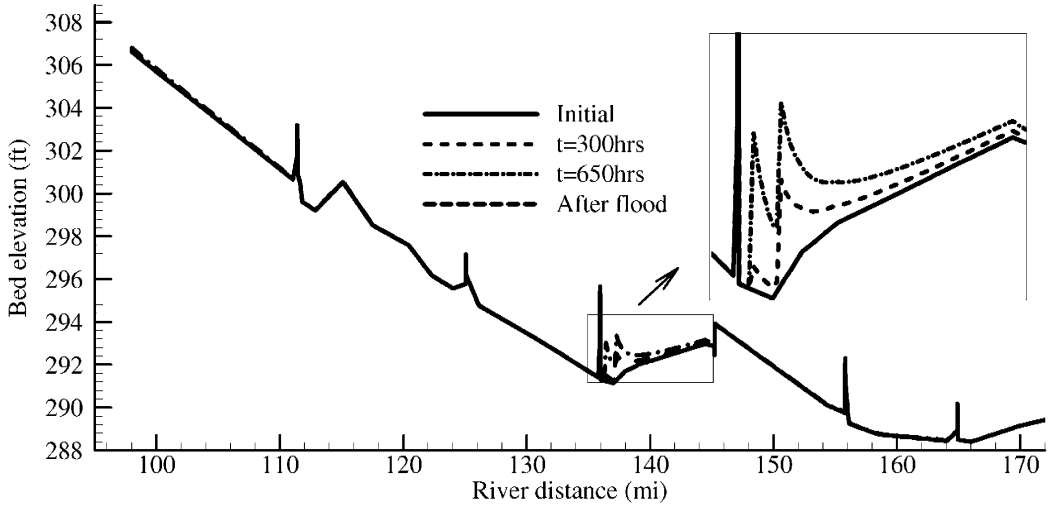

Figure 4.8. Bed elevation change of the SLC before and after a flood event.

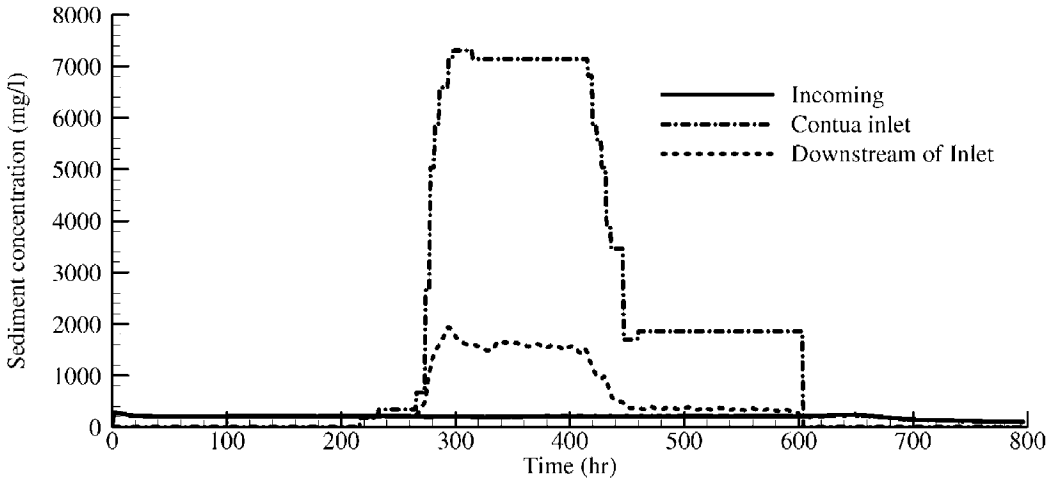

Figure 4.9. Sediment concentration changes with time at the four barrel inlet of the SLC.

4.5 Summary

Considerable advances in predicting cohesive sediment transport and related water quality have been made in the past decade. There are several numerical models that can be used to predict cohesive sediment transport movement, but they are subject to great uncertainty unless detailed measurements of important parameters can be made. In particular, it is necessary to measure the critical shear stresses for deposition and erosion. This chapter only summaries some basic processes involved in cohesive sediment transport. The methods summarized here are far from exhaustive.

It should also be noted that many traditional methods for non-cohesive sediment transport are also valid in cohesive sediment transport. For example, bathymetric analyses can be used to infer sediment movement, and geochronologic analyses can be used to age sediments. These types of field data collection are invaluable for validating numerical models.

4.6 References

Amos C.L., N. van Wagoner, and G.R. Daborn (1988). "The Influence of Subaerial Exposure on the Bulk Properties of Fine-Grained Intertidal Sediment From Minas Basin, Bay of Fundy," *Estuarine Coastal Shelf Sci.*, vol. 27, pp. 1-13.

Ariathurai, R. (1974). "A Finite Element Model for Sediment Transport in Estuaries," PhD dissertation, Univ. of California, Davis, California.

Ariathurai, R., and K. Arulanandan (1978). "Erosion Rates of Cohesive Soils," *Journal of the Hydraulics Division*, Proceedings of the ASCE, vol. 104, no. HY2, February, pp. 279-283.

Ariathurai, R., and Krone, R.B. (1976). "Finite element model for cohesive sediment transport," *Journal of Hydraulic Division*, ASCE, vol. 102, no 3, pp. 323-338.

Arulanandan, K., P. Loganathan, and R.B. Krone (1975). "Pore and Eroding Influences on Surface Erosion of Soil," *Journal. of the Geotechnical Engineering Division*, Proceedings of the ASCE, vol. 101 (GTI), pp. 51-66.

Atterberg, A. (1911). "Lerornas Förhallande till Vatten, deras Plasticitetsgränser och Plasticitetsgrader," ("The Behavior of Clays with Water, Their Limits of Palsticity and Their Degrees of Plasticity,") *Kungliga Lantbruksakademiens Handlingar och Tidskrift,* vol. 50, no. 2, pp. 132-158: also in *Internationale Mitteilungen für Bodenkunde*, vol. 1, pp. 10-43 ("Uber die Physikalische Bodenuntersuchung und über die Plastizität der Tone").

Bennett, R.H., N.R. O'Brien, and M.H. Hulbert (1991). "Determinants of Clay and Shale Microfabric Signatures: Processes and Mechanisms," in *Microstructure of Fine-grained Sediments, from Mud to Shale*, R. H. Bennett and M.R. Hulbert (eds.), Springer-Verlag, New York, New York.

Black, K.S. (1997). "Microbiological Factors Contributing to Erosion Resistance in Natural Cohesive Sediments," in *Cohesive Sediments*, N. Burt, R. Parker and J. Watts (eds.) John Wiley and Sons, pp. 231-244.

Boates, J.S., and P.C. Smith (1988). "Crawling Behaviour of the Amphipod *Corophium volutator* and Foraging by Semipalmated Sandpipers, *Calidris pusilla*," *Can. Journal of Zoology*, vol. 67, pp. 457-462.

Brekhovskikh, V.F., V.K. Debolsky, G.N. Vishnevskaya, and N.S. Zolotareva (1991). "Erosion of Cohesive Bottom Sediments: The Influence of the Benthos," *Journal of Hydraulic Research*, vol. 29, no. 2, pp. 149-160.

Burban, P.Y., Y.U. Xu, J. McNeil, and W. Lick (1990). "Settling Speeds of Flocs in Fresh Water and Seawater," *Journal of Geophysics Research*, vol. 95, no. 10, pp. 18213-18200.

Burt, T.N. (1990). "Cohesive Sediment and Physical Models," *Int. Conf. on Phys. Modeling of Transport*, MIT, Cambridge, Massachusetts.

Chapuis, R.P., and T. Gatien (1986). "An improved rotating cylinder technique for quantitative measurements of the scour resistance of clays," *Can. Geotechnical Journal*, vol. 23, pp. 83-87.

Cole, P., and G.V. Miles (1983). "Two-Dimensional Model of Mud Transport," *Journal of Hydraulic Engineering*, ASCE, vol. 109, no. 1, pp. 1-12.

Cormault, P. (1971). "Détermination Expérimentale du Débit Solide D'érosion Fins Cohésifs," 14e Congrés de l'A.I.R.H., Paris.

Cornelisse, J.M., H.P.J. Mulder, E.J. Houwing, H. Williamson, and G. Witte (1994). "On the Development of Instruments for In-Situ Erosion Measurements," in *Cohesive Sediments*, N. Burt, R. Parker, and J. Watts (eds.), John Wiley and Sons Ltd., pp. 175-186.

Daborn, G.R. (1993). "An Ecological Cascade Effect: Migratory Birds Affect Stability of Intertidal Sediments," *Limnology and Oceanography*, vol. 38, no. 1, pp. 225-231.

Delo, E.A. (1988). "The Behavior of Estuarine Muds During Tidal Cycles," *Rep. SR 138*, Hydraulic Research Station, Wallingford, UK.

Dennett, K.E., T.W. Sturm, A. Amirtharajah, and T. Mahmood (1998). "Effects of Adsorbed Natural Organic Matter on the Erosion of Kaolinite Sediments," *Water Environment Research*, vol. 70, no. 3, pp. 268-275.

Fukuda, M.K., and W. Lick (1980). "The Entrainment of Cohesive Sediments in Fresh Water," *Journal of Geophysical Research*, vol. 85, no. C5, pp. 2813-2824.

Gailani, J., C.K. Ziegler, and W. Lick (1991). "Transport of Suspended Solids in the Lower Fox River," *Journal of Great Lakes Research*, vol. 17, no. 4, pp. 479-494.

Gust, G., and M.J. Morris (1989). "Erosion Thresholds and Entrainment Rates of Undisturbed In-Situ Sediments," Journal of Coastal Research, Special Issue 5, Ft. Lauderdale, Florida.

Hamrick, J. (2001). "EFDC1D, A One Dimensional Hydrodynamic and Sediment Transport Model for River and Stream Networks - Model Theory and Users Guide," Tetra Tech, Inc., Fairfax, Virginia.

Hayter, E.J. (1983). "Prediction of Cohesive Sediment Movement in Estuarial Waters," Ph.D. Thesis, the University of Florida at Gainesville.

Hayter, E.J., and C.V. Pakala (1989). "Transport of Inorganic Contaminants in Estuarial Water," *Journal of Coastal Research*, Special Issue, no. 5, pp. 217-230.

Hayter, E.J., M.A. Bergs, R. Gu, S.C. McCutcheon, S.J. Smith, and H.J. Whiteley (1999). "HSCTM-2D, A Finite Element Model for Depth-Averaged Hydrodynamics, Sediment and Contaminant Transport," Report, National Exposure Research Laboratory, Office of Research and Development, U.S. EPA, Athens, Georgia.

Hicklin, P.W., and P.C. Smith (1984). "Selection of Foraging Sites and Invertebrate Prey by Migrant Palmated Sandpipers *Caldris pusilla* in Minas Basin, Bay of Fundy," *Can. Journal of Zoology*, vol. 62, pp. 2201-2210.

Hilldale, R.C. (2001). "Fluvial Erosion of Cohesive Sediments Considering Turbulence and Secondary Flow," M.S. Thesis, Dept. of Civil and Environmental Engineering, Washington State University, Pullman, Washington.

Houwing, E.J., and L.C. van Rijn (1995). "In-Situ Determination of the Critical Bed Shear Stress for Erosion of Cohesive Sediments," *Proceedings of the Coastal Engineering Conference*, vol. 2, Kobe, Japan, October 1994, pp. 2058-2069.

Hwang, K.N., and A.J. Mehta (1989). "Fine Sediment Erodibility in Lake Okeechobee," Coastal and Oceanographic Engineering Dept., Univ. of Florida, Report UFL/COEL-89/019, Gainesville, Florida.

Johansen, C., T. Larsen, and O. Petersen (1997). "Experiments on Erosion of Mud From the Danish Wadden Sea," in *Cohesive Sediments*, N. Burk, R. Parker, and J. Watts (eds.), John Wiley & Sons, pp. 305-314.

Kamphuis, J.W., and K.R. Hall (1983). "Cohesive Material Erosion by Unidirectional Current," *Journal of Hydraulic Engineering*, vol. 109, no. 1, January, pp. 49- 61.

Kelly, W.E., and R.C. Gularte (1981). "Erosion Resistance of Cohesive Soils," *Journal of the Hydraulics Division*, Proceedings of the ASCE, vol. 107, no. HY10, October, pp. 1211-1224.

Klumpp, C., J. Huang, and B.P. Greimann (2003). "Sediment Model of the Arroyo Pasajero and California Aqueduct," Bureau of Reclamation Report prepared for the CA Dept. of Water Resources, in preparation. (still in preparation)?

Kuijper, C., J.M. Cornelisse, and J.C. Winterwerp (1989). "Research on Erosive Properties of Cohesive Sediments," *Journal of Geophysical Research*, vol. 94, no. 10, October, pp. 14341 – 14350.

Krishnappan, B.G. (1993). "Rotating Cylinder Flume," *Journal Hydraulic Engineering*, vol. 119, no. 6, pp. 758-767.

Krone, R.B. (1962). "Flume Studies of the Transport of Sediment in Estuarial Shoaling Processes," Technical Report, Hydraulic Engineering Laboratory, University of California, Berkeley California.

Laursen, E.M. (1958). "The total sediment load of streams," *Journal of Hydraulic Division, ASCE*, vol. 84(1), pp. 1531-1536.

Letter, J.V., B.P. Donnell, W.H. McAnally, and W.A. Thomas (2000). "Users Guide to SED2D WES version 4.5," U.S. Army, Engineer Research And Development Center, Waterways Experiment Station, Coastal and Hydraulics Laboratory.

Li, M.Z., and C.L. Amos (1995). "SEDTRANS92: A Sediment Transport Model for Continental Shelves," *Computers and Geosciences*, vol. 21, no. 4, pp. 533-554.

Lick, W., and J. Lick (1988). "Aggregation and Disaggregation of Fine-Grained Lake Sediments," *Journal of Great Lakes Research*, vol. 14, no. 4, pp. 514-523.

Maa, J.P.Y. (1989). "The Bed Shear Stress of an Annular Sea-Bed Flume," *Proc., Water Quality Management*, Hamburg, Germany, pp. 271-276.

Manzenrider, H. (1983). Retardation of Initial Erosion Under Biological Effects in Sandy Tidal Flats. Leichtweiss, Inst. Tech. University Branschweig, 423 -435.

Masch, F.D., W.H. Espey Jr., and W.L. Moore (1963). "Measurements of the Shear Resistance of Cohesive Sediments," *Proceedings of the Federal Inter-Agency Sedimentation Conference*, Agricultural Research Service, Publication No. 970, Washington DC., pp. 151-155.

McAnally, W.H., and A.J. Mehta (2001). "Collisional Aggregation of fine Estuarial Sediment," Coastal and Estuarine Fine Sediment Processes, *Proceedings in Marine Science 3.*

McNeil, J., C. Taylor, and W. Lick (1996). "Measurements of Erosion of Undisturbed Bottom Sediments With Depth," *Journal of Hydraulic Engineering*, vol. 122, no. 6, pp. 316-324.

Meadows, P.S., and A. Meadows (1991). *The Environmental Impact of Burrows and Burrowing Animals,* Proceedings of a Symposium of the Zoological Society of London, Clarendon Press, Oxford.

Meadows, P.S., and J. Tait (1985). "Bioturbation, Geotechnics and Microbiology at the Sediment-Water Interface in Deep Sea Sediments," *Proceedings of the 19th European Marine Biology Symposium,* Gibbs, P.E. (ed.), Cambridge University Press, pp. 191-199.

Meadows, P.S., and J. Tait (1989). "Modification of Sediment Permeability and Shear Strength by Two Burrowing Invertebrates," *Marine Biology*, vol. 101, pp. 75-82.

Meadows, P.S., J. Tait,, and S.A. Hussain (1991). "Effects of Estuarine Infauna on Sediment Stability and Particle Sedimentation," *Hydrobiologia*, vol. 190, pp. 263-266.

Mehta, A.J., and E. Partheniades (1973). "Depositional Behavior of Cohesive Sediments," *Tech report No. 16*, Univ. of Florida, Gainesville, Florida.

Mehta, A.J., E.J. Hayter, W.R. Parker, R.B. Krone, and A.M. Teeter (1989). "Cohesive Sediment Transport. I: Process Description," *Journal of Hydraulic Engineering*, vol. 115, no. 8, pp. 1076-1093.

Millar, R.G., and M.C. Quick (1998). "Stable width and depth of gravel bed rivers with cohesive banks," *Journal of Hydraulic Engineering*, vol. 124(10), 1005-1013.

Molinas, A., and C.T. Yang (1985). "Generalized water surface profile computations," *Journal of the Hydraulic Diversion, ASCE*, vol. 111, no. HY3, pp. 381-397.

Moody, L.F. (1944). "Friction Factors for Pipe Flow," *Trans. ASME*, vol. 66.

Nachtergaele, J., and J. Poesen (2002). "Spatial and Temporal Variations in Resistance of Loess-Derived Soils to Ephemeral Gully Erosion," *European Journal of Soil Science*, vol. 53, September, pp. 449-463.

Nezu, I., and H. Nakagawa (1993). "*Turbulence in Open-Channel Flows,*" International Association for Hydraulic Research, Monograph Series, A.A. Balkema, Rotterdam, The Netherlands.

Nicholson, J., and B.A. O'Connor (1986). "Cohesive Sediment Transport Model," *Journal of Hydraulic Engineering*, vol. 112, no. 7, pp. 621-640.

Odd, N.V.M., and M.W. Owen (1972). "A Two-Layer Model for Mud Transport in the Thames Estuary," *Proc. of the Institution of Civil Engineers*, London, Supplement (ix), pp. 175-205.

Onishi, Y. (1981). "Sediment-Containment Transport Model," *Journal of Hydraulic Division*, ASCE, vol. 107, no. 9, pp. 1089-1107.

Parchure, T.M., and A.J. Mehta (1985). "Erosion of Soft Cohesive Sediment Deposits," *Journal of Hydraulic Engineering*, ASCE, vol. 111, no. 10, October, pp. 1308-1326.

Partheniades, E. (1962). *A Study of Erosion and Deposition of Cohesive Soils in Salt Water*, Ph.D. Thesis, University of California, Berkeley.

Partheniades, E. (1965). "Erosion and Deposition of Cohesive Soils," *Journal of the Hydraulics Division, Proceedings of the ASCE*, vol. 91, no. HY1, January, pp. 105-139.

Partheniades, E., J.F. Kennedy, R.J. Etter, and R.P. Hoyer (1966). "Investigations of the Depositional Behavior of Fine Cohesive Sediments in an Annular Rotating Channel.," *Hydrodynamics Lab Report No. 96*, MIT, Cambridge Massachusetts.

Paterson, D.M. (1994). "Microbiological Mediation of Sediment Structure and Behaviour," in *Microbial Mats* NATO ASI, vol. G 35, P Caumette and L.J. Stal (eds.), Springer-Verlag, pp. 97-109.

Paterson, D.M. (1997). "Biological Mediation of Sediment Erodibility: Ecology and Physical Dynamics," in *Cohesive Sediments,* N. Burt, R. Parker, and J. Watts (eds.), John Wiley and Sons, pp. 215-229.

Paterson, D.M., and G.R. Daborn (1991). "Sediment Stabilization by Biological Action: Significance for Coastal Engineering," in *Developments in Coastal Engineering,,* Peregrine, D. H. and J.H. Loveless (eds.), University of Bristol Press, pp. 111-119.

Raudkivi, A.J. (1998). *Loose Boundary Hydraulics*, A.A. Balkema, Rotterdam, The Netherlands, pp. 271-311.

Ravens, T.M., and P.M. Gschwend (1999). "Flume Measurements of Sediment Erodibility in Boston Harbor," *Journal of Hydraulic Engineering*, vol. 125, no. 10, pp. 998-1005.

Ravisanger, V., K.E. Dennett, T.W. Sturm, and A. Amirtharajah (2001). "Effect of Sediment pH on Resuspension of Kaolinite Sediments," *Journal of Environmental Engineering*, vol. 127, no. 6, June, pp. 531-538.

Roberts, J, R. Jepsen, D. Gotthard, and W. Lick (1998). "Effects of Particle Size and Bulk Density on Erosion of Quartz Particles," *Journal of Hydraulic Engineering*, vol. 124, no. 12, pp. 1261-1267.

Scarlatos, P.D. (1981). "On the Numerical Model of Cohesive Sediment Transport," *Journal of Hydraulic Research*, vol. 19, no. 1, pp. 61-68.

Schnitzer, M., and S.U. Khan (1972). *Humic Substances in the Environment*, Marcel Dekker, New York, New York.

Sheng, Y.P. (1983). Mathematical Modeling of Three-Dimensional Coastal Currents and Sediment Dispersion: Model Development and Application, technical report CERC-83-2, U.S. Army WES, Vicksburg, Mississippi.

Sheng, Y.P. (1988). "Consideration of Flow in Rotating Annuli for Sediment Erosion and Deposition Studies," *Journal of Coastal Research*, vol. S15, pp. 207-216.

Sheng, Y.P. (1986). "A Three-Dimensional Mathematical Model of Coastal, Estuarine and Lake Currents Using Boundary-Fitted Grid," Report No. 585, A.R.A.P. Group of Titan Systems, Princeton, New Jersey.

Sherard, J.L., R.S. Decker, and N.L. Ryka (1972). "Piping in Earth Dams of Dispersive Clay," presented at the ASCE Soil Mechanics and Foundation Conference, Perdue University, Lafayette, IN, June 12-14.

Shrestha, P.L., and G.T. Orlob (1996). "Multiphase Distribution of Cohesive Sediments and Heavy Metals in Estuarine Systems," *Journal of Environmental Engineering*, ASCE, vol. 122, no. 8, pp. 730-740.

Smerdon, E.T., and R.P. Beasley (1959). "The Tractive Force Theory Applied to Stability of Open Channels in Cohesive Soils," *Research Bulletin 715*, University of Missouri Agricultural Experiment Station, Columbia, Missouri.

Spasojevic, M., and F.M. Holly (1996). "Cohesive Sediment Capability in CH3D Phases II and III: Formulation and Implementation," IIHR Report no. 386, Iowa Institute of Hydraulic Research, The University of Iowa, Iowa City, Iowa.

Teisson, C., and B. Latteux (1986). "A Depth-Integrated Bidimensional Model of Suspended Sediment Transport," Proceedings., 3d International Symposium On River Sedimentation, S.Y. Wang, H.W. Shen, and L.Z. Ding (eds.), Jackson, MS, pp. 421-429.

Teisson, C., M. Ockenden, P. Le Hir, C. Kraneberg, and L. Hamm (1993). "Cohesive Sediment Transport Processes," *Coastal Engineering,* Elsevier Publishers, vol. 21, pp. 129-162.

Tetra Tech, Inc. (2000). "EFDC Technical Memorandum: Theoretical and Computational Aspects of Sediment Transport in the EFDC Model, 2nd Draft," Tetra Tech, Inc., Fairfax, Virginia.

Thomann, R.V., and D.M. DiToro (1983). "Physico-Chemical Model of Toxic Substances in the Great Lakes," CR805916 and CR 807853, U.S. Environmental Protection Agency (EPA), Large Lakes Res. Station, Grosse Isle, Michigan.

Thorn, M.F.C. (1981). "Physical Processes of Siltation in Tidal Channels," *Proceedings of the Conference on Hydraulic Modelling Applied to Maritime Engineering Problems*, Institution of Civil Engineers, London, England, 1981, pp. 47-55.

Thorn, M.F.C., and J.G. Parsons (1977). "Properties of Grangemouth Mud," Report No. EX 781, Hydraulics Research Station, Wallingford, England, July.

Thorn, M.F.C., and J.G. Parsons (1980). "Erosion of Cohesive Sediments in Estuaries," *Third Int. Symp. On Dredging Technology*, Bordeaux, France.

Thurman, E.M., and R.L. Malcolm (1983). "Structural Study of Humic Substances: New Approaches and Methods," in *Aquatic and Terrestrial Humic Substances,* R.F. Christman and E.T. Gjessing (eds.), Ann Arbor Science, Ann Arbor, Michigan.

U.S. Army Corps of Engineers (1993). The Hydraulic Engineering Center, *HEC-6 Scour and Deposition in Rivers and Reservoirs, User's Manual,* March 1977 (revised 1993).

van Leussen, W. (1994). "Estuarine Macroflocs and Their Role in Fine-Grained Sediment Transport," "Ph.D. thesis, Utrecht University (NL).

van Rijn, L. (1993). Principles of Sediment Transport in Rivers, Estuaries and Coastal Seas, Aqua Publications, The Netherlands.

Vermeyen, T. (1995). "Erosional and Depositional Characteristics of Cohesive Sediments Found in Elephant Butte Reservoir, New Mexico," Technical Report R-95-15, Water Resources Services, Technical Service Center, Bureau of Reclamation, Denver, CO.

Verwey, E.J.W., and J.T.G. Overbeek (1948). *Theory of the Stability of Hydrophobic Colloids*, Elsevier Publishing Co., New York, New York.

Westrich, B., R. Scharf, and V. Schürlein (1997). "Measurement of Cohesive Sediment Erodibility in a Laboratory Flume," *Environmental and Coastal Hydraulics: Protecting the Aquatic Habitat*, Proceedings of the 27th Congress of the IAHR, Part B-1, Aug. 10-15, San Francisco, pp. 209-215.

Winterwerp, J.C., J.M. Cornelisse, and C. Kuijper (1990). "Parameters to Characterize Natural Muds," in Abstract Volume, Int. Workshop on Cohesive Sediments, Brussels, KBIN, Brussels, 103-105.

Winterwerp, J.C., J.M. Cornelisse, and C. Kuijper (1993). "A Laboratory Study on the Behavior of Mud from the Western Scheldt Under Tidal Conditions," *Coastal and Estuarine Studies*, vol. 42, Nearshore and Estuarine Sed. Transport, AGU.

Yang, C.T., and F.J.M. Simões (2000). User's Manual for GSTARS 2.1 (Generalized Sediment Transport model for Alluvial River Simulation version 2.1), Bureau of Reclamation, Technical Service Center, Denver, Colorado.

Yang, C.T., and F.J.M. Simões (2002). *User's Manual for GSTARS3 (Generalized Sediment Transport Model for Alluvial River Simulation version 3.0),* Bureau of Reclamation, Technical Service Center, Denver, Colorado.

Yang, C.T., J. Huang, and B.P. Greimann (2004, 2005). *User's manual for GSTAR-1D (Generalized Sediment Transport model for Alluvial Rivers - One Dimension)*, version 1.0, U.S. Bureau of Reclamation, Technical Service Center, Denver, Colorado.

Young, R.A., and J.B. Southard (1978), "Erosion of Fine-Grained Sediments: Seafloor and Laboratory Experiments," *Bulletin of the American Geological Society*, vol. 89, pp. 663-672.

Ziegler, C.K., and W. Lick (1986). "A Numerical Model of the Resuspension, Deposition and Transport of Fine-Grained Sediments in Shallow Water," UCSB Rep. ME-86-3, University of California, Santa Barbara, California.

Ziegler, C.K., and B.S. Nisbet (1994). "Fine-Grained Sediment Transport in Pawtuxet River, Rhode Island," *Journal of Hydraulic Engineering*, ASCE, vol. 120, no. 5, pp. 561-576.

Ziegler, C.K., and B.S. Nisbet (1995). "Long-Term Simulation of Fine-Grained Sediment Transport in a Large Reservoir," *Journal of Hydraulic Engineering*, vol. 121, no. 11, pp. 773-781.

Zreik, D.A., B.G. Krishnappan, J.T. Germaine, O.S. Madsen, and C.C. Ladd (1998). "Erosional and Mechanical Strengths of Deposited Cohesive Sediments," *Journal of Hydraulic Engineering*, vol. 124, no. 11, pp. 1076 – 1085.